Ministry for Primary Industries
Manatū Ahu Matua

Distributions of water mass, water quality and sea ice during the New Zealand IPY-CAML survey of the Ross Sea

New Zealand Aquatic Environment and Biodiversity Report No. 133

J.N. Schwarz,
M. Williams,
M. Walkington,
H. Chang,
E. Maas,
C. Stephens,
M. Gall,
M.H. Pinkerton,
C. Cunningham,
J. Hall

ISSN 1179-6480 (online)
ISBN 978-0-478-43266-4 (online)

July 2014

New Zealand Government

Growing and Protecting New Zealand

Requests for further copies should be directed to:

Publications Logistics Officer
Ministry for Primary Industries
PO Box 2526
WELLINGTON 6140

Email: brand@mpi.govt.nz
Telephone: 0800 00 83 33
Facsimile: 04-894 0300

This publication is also available on the Ministry for Primary Industries websites at:
http://www.mpi.govt.nz/news-resources/publications.aspx
http://fs.fish.govt.nz go to Document library/Research reports

TABLE OF CONTENTS

EXECUTIVE SUMMARY

Schwarz, J.; Williams, M.; Walkington, M.; Chang, H.; Maas, E.; Stephens, C.; Gall, M.; Pinkerton, M.; Cunningham, C.; Hall, J. (2014). Distributions of water mass, water quality and sea ice during the New Zealand IPY-CAML survey of the Ross Sea.

***New Zealand Aquatic Environment and Biodiversity Report No. 133.* 36 p.**

Objective 4 of project IPY200701 addressed the background physical and surface biological conditions at the time of the New Zealand IPY-CAML survey of the Ross Sea (February–March 2008). Objective 4 was split into two parts: A, characterisation of the biological environment and bio-optical regime using continuous underway sampling, and B, identification of fronts using discrete and underway sampling of temperature, salinity and nutrient profiles.

The IPY voyage covered mostly Antarctic Surface Water. Two prominent phytoplankton blooms were observed, in which nitrate:phosphate ratios were constant suggesting that nutrients were replete, yet there were some optical indications of phytoplankton senescence. Dense, high salinity, subsurface shelf waters were sampled in only a few stations, while Modified Circumpolar Deep Water was sampled at all shelf and deep-water stations. The range of physical characteristics and locations of surface frontal expressions were consistent with the literature.

However passive microwave satellite data indicated that sea-ice concentrations were unusually high during both months of the voyage, compared to the nine-year AMSR- E mean, and a significant, though spatially variable correlation was found between ice cover anomaly and the Southern Oscillation Index.

Novel bio-optical data were gathered during the voyage. Although quality control of optical scattering measurements was difficult, a useful volume of data was collected for comparison with ocean colour satellite imagery. The spatial coverage of the satellite data during the period of the voyage was severely inhibited by cloud and ice cover. The voyage dataset therefore lends itself to an examination of bias in the monthly composites of satellite-derived chlorophyll and primary production values, which are commonly used to examine primary production.

Differences between temperature and salinity data from different equipment were confounded by drifting of the ship between deployments. However, in many cases differences were less than 0.001 in both temperature and salinity, indicating that these alternative datasets yield useful information, expanding the coverage of temperature and salinity measurements. As the DTIS sensor was trawled for several kilometres on each deployment, this dataset also provides valuable information about spatial variability in temperature and salinity in the deeper water masses, although the analysis of this information is beyond the scope of this report.

SPECIFIC OBJECTIVE 4A:

To characterise the physico-chemical environment by collecting bio-optical data underway to allow ground-truthing of remotely-sensed measurements from ocean colour satellites.

SPECIFIC OBJECTIVE 4B:

To analyse spot salinity, temperature and nutrient profiles, and analysing underway salinity and temperature data to identify fronts.

1. METHODS

1.1 Objective 4A

A new underway water analysis system was fitted to the R.V. *Tangaroa* for the IPY voyage with water intakes in the bow and through the sea-chest amidships at a depth of approximately 7 m. The system was operated continuously. Temperature was measured using a SeaBird thermosalinograph SBE-38 for the bow water intake, which was positioned very close to the water with less than 1 minute delay between intake and measurement. Temperature and salinity were measured using a SeaBird SBE-21 for the main underway system amidships. This latter system incorporated a Wetlabs Eco-triplet, measuring in vivo chlorophyll fluorescence, fluorescence by coloured, dissolved organic matter (CDOM) and backscatter at a wavelength of 660 nm; a Wetlabs transmissometer with 25 cm pathlength, measuring beam attenuation at 660 nm and the volume scattering coefficients at 3 angles and wavelengths of 432 nm, 530 nm, 660 nm using a Wetlabs-VSF3. The optical sampling windows were cleaned daily using purified water. The Wetlabs-VSF3 backscatter data were despiked to remove the influence of occasional large particles. Manufacturer's calibrations were applied to all instruments. The Turner in vivo fluorometer ceased to function during the return transit from the Ross Sea to New Zealand and the data are neglected here in favour of the Ecotriplet.

Water samples were collected from the underway flow during transit, for biological and chemical analysis. Phytoplankton absorption was measured using a Perkin Elmer spectrophotometer after Tassan & Ferrari (1995). Because of the loss of chlorophyll sample filters due to freezer malfunction, the absorption filters were used immediately after absorption measurements for pigment analysis. Phytoplankton pigments were extracted in HPLC-grade acetone by sonication and overnight storage at -20°C. Pigments were analysed using High Performance Liquid Chromatography (HPLC) after Zapata et al. (2000). The analysis was carried out on a Phenomenex Luna 3u C8 (2) column with photo-diode array (350–800 nm) and fluorescence (435 ex, 670 em) detection. Standard calibration curves were produced using Sigma™ Chlorophyll-a, chlorophyll-b, lutein, beta-beta-carotene; Fluka™APO; DHI™ chlorophyll-c3, chlorophyll-c2, peridinin, fucoxanthin, prasinoxanthin, diadinoxanthin, 19'-hexanoloxyfucoxanthin, myxoxanthin and alloxanthin. Other pigments were quantified following Jeffrey et al. (1997). Pigments were identified by retention time and absorption spectrum. Chlorophyll-a was also measured fluorometrically using a Cary Ellipse fluorometer, calibrated against a chlorophyll-a standard and verified spectrophotometrically using a Perkin Elmer spectrophotometer (Parsons et al. 1992). This is termed "in vitro fluorescence" and is distinguished from in vivo fluorescence where measurement is made on intact cells rather than on phytoplankton pigments extracted into an organic solvent. Particulate organic carbon and nitrogen were analysed by catalytic combustion at 900°C, using a CE Instruments C/N analyser. Nutrients (nitrate+nitrite, ammonia and dissolved, reactive phosphate) were measured using an Astoria auto-analyser with periodic calibration against standards. Phytoplankton taxonomy is described in Stephens et al. (2010).

Bathymetry data were taken from the ETOPO 1 arc-minute integrated relief model (Amante & Eakins 2009). These data were used to aid interpretation of the in situ measurements.

1.2 Objective 4B

In addition to the thermosalinographs mounted within the underway system described in Section 1.1, a conductivity-temperature-depth (CTD) profiler was deployed for station work. This was a Seabird SBE 911 with Wetlabs transmissometer and fluorometer fitted. It was deployed with twenty four 12-litre Niskin bottles for water sampling.

In order to measure temperature and salinity with sufficient accuracy to identify water masses and determine mixed layer depths, several criteria must be met:

- The sensors must be immersed prior to profiling for a sufficient length of time for the sensor internal temperatures to equilibrate.
- Pairs of temperature and salinity sensors must be used to provide quality control - for identification of water masses, the difference between measurements made by the sensor pair must be much less than the differences in temperature and salinity between the water masses to be identified.
- The surface of the salinity probe, the pump which circulates water between the paired temperature and salinity sensors and the tubing connecting the sensors must be free of ice.

During the IPY voyage, problems with sensors freezing on deck meant that in many cases these criteria were not all met, with the result that much data did not meet acceptable standards and were discarded during standard processing. To maximise the temperature-salinity data coverage, a detailed quality analysis was carried out, comparing the CTD data with MOCNESS (Stephens et al., 2010) and DTIS (Bowden et al. 2011) deployments, both of which included Seabird SBE38 microcats which were used as CTDs. This is discussed in Section 1.3 below.

Three types of sampling were undertaken on station during the voyage. These are referred to in the remainder of this report as:

- AE: Acidification Experiments (Hanchet et al. 2008 section 5.4.3).
- ICOMM: International Census of Marine Microbes (Stephens et al. (2010), Maas et al., in prep.)
- Core: Core CTD profile stations (Hanchet et al. 2008).

Water masses were classified according to Jacobs & Giulivi (1998) and Smethie & Jacobs (2005). The typical physical characteristics of each water mass are summarised in Table 1. To aid interpretation, Figure 1 illustrates schematically the interactions between water masses around the Antarctic continent.

Discrete station locations are shown in Figure 2. No reliable physical oceanography data were obtained for the AE stations (see Stephens et al., 2010). Biological and physical water analyses for the discrete stations were performed as described in Section 1.1.

Table 1: Water mass classifications used for the IPY voyage, taken from Jacobs & Giulivi, (1998).

Water mass	Temp-erature	Salinity	Depth range	Lat/Lon	Notes
Antarctic Intermediate Water (AAIW)	3 to 7°C	34.2 to 34.4	700 to 1200 m	~ 50–60°S – formed at Polar Front, transported northwards	Salinity increases beyond range as water moves northward
Circumpolar Deep Water (CDW)	~ 1.3°C	~ 34.7	~300 m to bottom	~ south of the Polar Front	Rises from the sub-tropical mid-depths; O_2 poor
Antarctic Surface Water (AASW)	<2.0°C	<34.5	Surface	South of the Polar Front	Formed as meltwater mixes with surface waters
Antarctic Bottom Water (AABW)	-0.8 to 0.04°C	34.66 to 34.71	Close to sea floor	Throughout study region	Formed by mixing of HSSW and CDW
Sub-Antarctic Water (SAW)	>8.0°C	>34.5	Surface	North of the Sub-Antarctic Front	
Modified Circumpolar Deep Water (MCDW)	-1.5 to 1.0°C				Formed by mixing of CDW and AASW across the ASF
High Salinity Shelf Water (HSSW)	~ -1.9°C	>34.6	< 1000 m	On the shelf	Mixes with CDW to form AABW

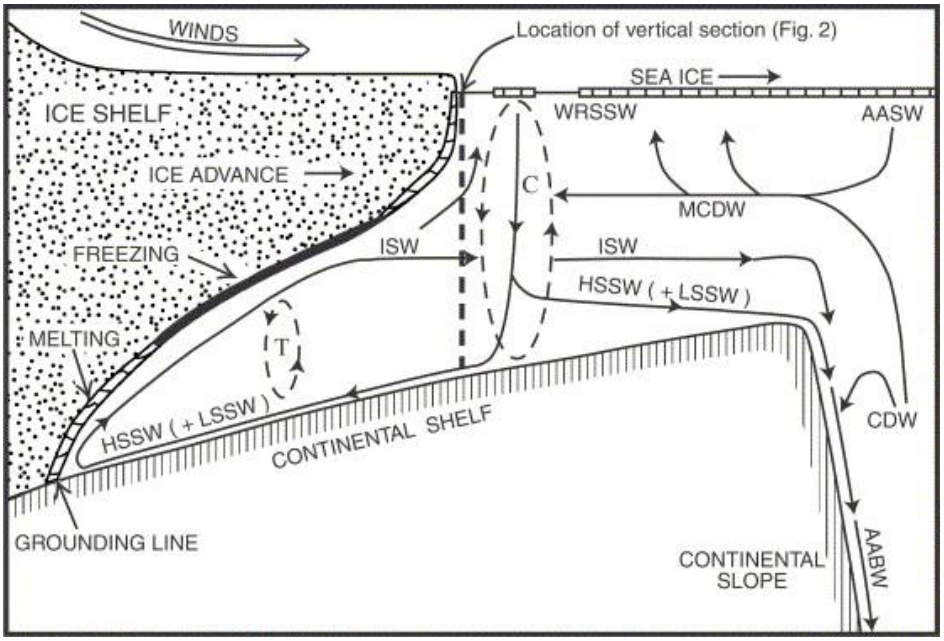

Figure 1: Water mass formation and interactions in the Ross Sea (reproduced from Smethie & Jacobs, 2005).

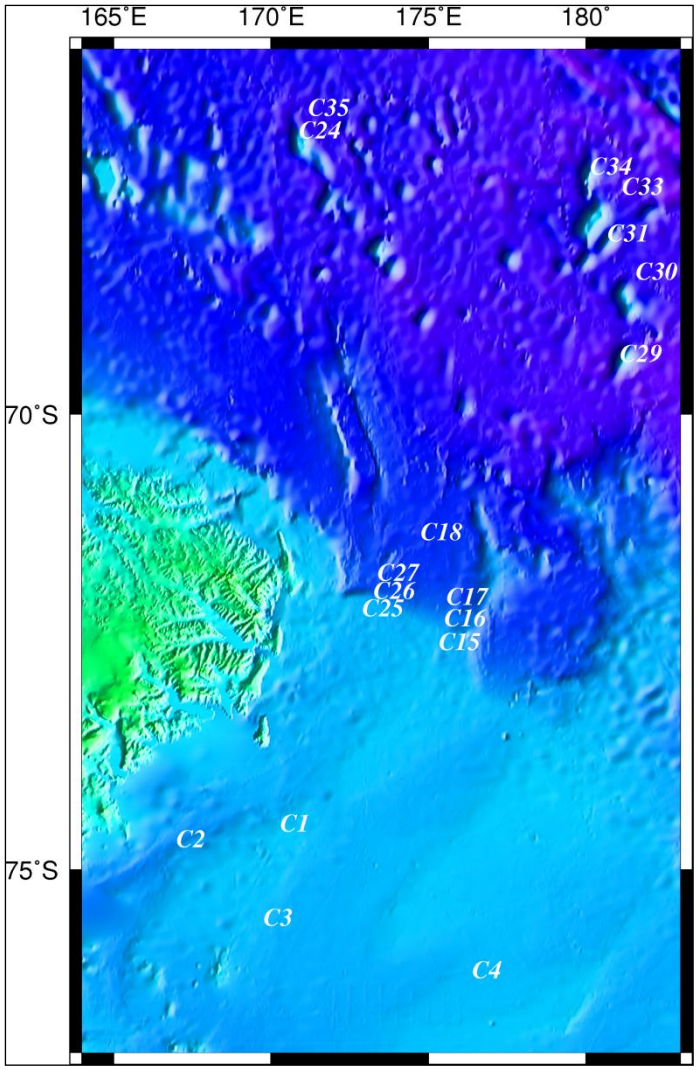

Figure 2: Location of core stations.

1.3 CTD Intercomparison

CTD-rosette Profiles

Tables 3 and 4 detail the different sensor deployment locations for core and ICOMM stations. Note the very great distances between ICOMM stations and MOCNESS/DTIS deployments. For the Microcat instruments, only upcasts were selected to avoid periods when the sensors had not temperature-equilibrated. For the CTD, as upcasts were carried out with faster winch speeds, the sample density would have been too low, so only CTD downcasts were used. Low sample rates were particularly problematic at the strong gradients of the pycnocline and introduced uncertainty into derivations of mixed layer depth.

CTD data were supplied by Matt Walkington (NIWA) having been calibrated but not quality controlled (by request). They were then processed using Matlab script ipy_ctd_intercomparison.m (available on the Project drive). The processing steps were:

1. Stations with very bad data or only 20 m data were ignored: u5407, u5408, u5409, u5410, u5413, u5422, u5425.

2. Single spikes were removed by seeking points which differed from the two neighbouring points above and below them by the values given in Table 2
3. Oxygen values less than 60 were set to NotANumber (NaN).
4. Data collected in air were removed.
5. Depth in metres was calculated using latitude and pressure (Matlab: seawater library).
6. Data values were binned to 1 m intervals, using the median value, instead of the mean, to minimise bias from remaining spikes.
7. Beam attenuation values more than 5 were set to NotANumber (NaN).
8. Using plots of temperature and salinity from the second sensor pair (t2, s2 in Matt Walkington's original data files - these performed better than the first pair sensors) - remaining spikes in temperature and salinity were identified by hand and set to NotANumber (NaN).
9. Difference between sensor pairs were calculated, together with potential temperature, potential density and buoyancy frequency.
10. Data were output to text and matlab files, one file per station.
11. Mat-files were passed to Mike Williams (NIWA) for calculation of mixed layer depth before step 8 had been performed.

Table 2: Despiking thresholds for this processing and for WOCE processing (WOCE values taken from http://cdiac.ornl.gov/ftp/oceans/a06woce/a06do.txt).

Parameter	Spike threshold	WOCE spike threshold
Pressure	3 dbar	0.5 db
Salinity	0.1 psu	0.032 mS/cm conductivity below 1500 dbar; 0.005 mS/cm above 1500 dbar.
Temperature (P > 1500 db)	0.1 °C	0.005 °C
Temperature (P < 1500 db)	0.5 °C	0.032 °C
Chlorophyll fluorescence	0.1 arbitrary units	n/a
Beam attenuation	0.02 m^{-1}	n/a
Oxygen	5 arbitrary units	n/a

MOCNESS and DTIS Microcat TS sensors

DTIS data measured during transects required less aggressive quality control, because the sensor had ample time to equilibrate during the approximately 2 hour deployments. DTIS up- and downcasts were carried out rather rapidly, yielding poor depth resolution (about 1–2 m or more).

DTIS/Trawl temperature and salinity data processing:

- Data collected at depths less than 3 m were removed to avoid partial air-water sampling periods.
- Upcasts were identified by screening for the first instance of ten consecutive depth values which were successively shallower by 1 m or more.
- For stations up to Station 180, the resulting depth, temperature, salinity triplets were output to new mat-file and text file (for these deployments, the computer internal time was set to 1980 and thus not accurate).
- For stations later than Station 180, the time-stamp for each row of data was used to query the ship's underway navigation for latitude and longitude.

- The distance between the start and end of the deployment was calculated for reference.
- The Matlab formatted time-stamp, latitude, longitude, temperature, salinity and depth data were output to the new mat-file and text file.

MOCNESS data were treated in the same way as the DTIS data. All of the MOCNESS data could be referenced to ship's position using the time stamps.

Table 3: Positions of AE and ICOMM stations together with details of the closest CTD, DTIS and MOCNESS stations. Note that none of the DTIS, trawl or MOCNESS stations is closer than 240 km to the CTD station location.

AltStnName	Julianday	StnLat	StnLon	ClosestCTD	CTDStnNo	CTDLat	CTDLon	CTDDistance	ClosestMOCStnNo	MOCJDay	MOCLat	MOCLon	MOCDistance	ClosestDTISStnNo	DTISJDay	DTISLat	DTISLon	DTISDistance
AE1	34	-52.9227	174.8158	NaN	3	NaN	NaN	NaN	283	72	-66.6985	171.3174	1545.37	294	73	-66.5532	170.5906	1534.89
ICOM55	34	-55.0105	174.7983	5402	5	-55.0102	174.798	0	283	72	-66.6985	171.3174	1314.21	294	73	-66.5532	170.5906	1304.39
ICOM60	35	-59.9887	175.5583	5403	8	-59.9887	175.559	0	283	72	-66.6985	171.3174	775.94	294	73	-66.5532	170.5906	771.34
AE2	36	-63.4477	178.534	5404	10	-63.4478	178.536	0	238	68	-67.3785	-179.8653	443.77	255	68	-67.2026	179.5591	420.68
ICOM65	37	-65.0065	179.9735	5405	12	-65.0062	180.026	0	238	68	-67.3785	-179.8653	264.15	255	68	-67.2026	179.5591	245.18

Table 4: Positions of Core stations together with details of the closest CTD, DTIS and MOCNESS stations.

CoreStnName	Julianday	CoreLat	CoreLon	ClosestCTD	CTDStnNo	CTDLat	CTDLon	CTDDistance	ClosestMOCStnNo	MOCJDay	MOCLat	MOCLon	MOCDistance	ClosestDTISStnNo	DTISJDay	DTISLat	DTISLon	DTISDistance
C1	42	-74.5818	170.291	5406	23	-74.5817	170.291	0.01	42	43	-74.7625	167.0689	96.91	26	42	-74.3498	170.1072	26.40
C2	43	-74.7503	166.9862	5407	36	NaN	NaN	NaN	42	43	-74.7625	167.0689	2.78	66	45	-75.3825	167.1984	70.64
C3	44	-75.6158	169.7525	NaN	52	NaN	NaN	NaN	57	43	-75.6287	169.8503	3.06	56	45	-75.38	169.4314	27.73
C4	48	-76.1863	176.392	NaN	90	NaN	NaN	NaN	95	48	-76.209	176.1996	5.70	94	49	-76.1127	176.2118	9.50
C15	50	-72.5891	175.3247	5411	112	-72.589	175.325	0.01	122	48	-72.3424	175.495	28.05	115	51	-72.3424	175.1505	28.08
C16	52	-72.33	175.5042	NaN	118	NaN	NaN	NaN	122	48	-72.3424	175.495	1.41	115	51	-72.3424	175.1505	12.03
C17	53	-72.0938	175.5718	NaN	132	NaN	NaN	NaN	134	54	-72.0798	175.5083	2.68	133	53	-72.0857	175.2378	11.47
C27	54	-71.9447	173.3735	5414	143	-71.9462	173.371	0.18	156	56	-72.0195	173.2435	9.45	151	55	-72.0886	173.089	18.77
C26	54	-72.024	173.2548	5415	148	-72.0238	173.255	0.03	156	56	-72.0195	173.2435	0.63	151	55	-72.0886	173.089	9.17
C25	55	-72.0836	172.8902	5416	160	-72.0835	172.89	0.03	158	56	-72.0087	173.1005	11.03	151	55	-72.0886	173.089	6.83
C18	57	-71.3838	174.7445	5417	175	-71.3823	174.748	0.21	170	57	-71.3713	174.6858	2.51	167	56	-71.4659	173.4978	45.14
C29	60	-69.4283	181.0915	5418	179	-69.4283	181.092	0.01	194	63	-68.0854	-179.2606	150.16	183	60	-69.2307	181.2026	22.43
C30	61	-68.5295	181.58	5419	184	-68.5295	181.58	0.00	194	63	-68.0854	-179.2606	60.33	183	60	-69.2307	181.2026	79.51
C31	62	-68.1112	180.6807	5421	196	-68.1125	180.68	0.15	194	63	-68.0854	-179.2606	3.77	198	62	-68.0604	179.1812	62.55
C33	65	-67.599	181.1473	5423	226	-67.598	181.15	0.15	232	67	-67.6162	-178.9331	3.91	219	64	-67.4701	179.4549	73.41
C34	67	-67.3772	180.1293	NaN	241	NaN	NaN	NaN	238	68	-67.3785	-179.8653	0.27	248	67	-67.2474	179.5563	28.53
C24	69	-66.9827	170.892	5426	260	-66.9818	170.892	0.10	261	70	-66.9671	170.859	2.25	278	70	-67.0035	171.051	7.30
C35	71	-66.7315	171.1778	5427	282	-66.7315	171.177	0.02	283	72	-66.6985	171.3174	7.16	278	70	-67.0035	171.051	30.78

Differences between CTD Sensor Pairs 1 and 2 (temperature and salinity) are given in Table 5. Among the northerly AE and ICOMM stations, good agreement for both temperature and salinity was found at ICOM55 and ICOMM65. At the core stations, bad profiles had already been eliminated and of the remaining 12 stations, only C1 suffered poor salinity replicability (erroneously high salinity in sensor pair 1), and at C15 the median salinity difference exceeded acceptable standards (see Table 2).

Table 5: Differences in temperature (upper) and salinity (red, lower) between the two pairs of T,S sensors on the CTD.

CTD station	Station Name	Minimum T [S] difference	Maximum T [S] difference	Median T [S] difference	Median T [S] in profile
n/a	AE1			No CTD data at this station	
u5402	ICOMM55	0	0.0787	-0.0002	6.396
		0.0	65.05	-0.00065	34.091
u5403	ICOMM60	0	0.0876	0.00028	3.505
		0.00015	65.11	-64.96	34.006
u5404	AE2	20.5	21.1	-20.7	2.186
		29.17	30.04	29.76	33.93
u5405	ICOMM65	0	0.0141	-0.00035	1.015
		0.0003	0.0075	-0.0032	34.148
5406	C1	0	0.3316	-0.0014	-1.8744
		10.97	34.14	24.31	34.65
-	C2			No CTD data at these stations	
-	C3			No CTD data at these stations	
-	C4			No CTD data at these stations	
5411	C15	0	0.074	0.00015	-1.0497
		0	2.024	0.1752	34.47
-	C16			No CTD data at these stations	
-	C17			No CTD data at these stations	
5414	C27	0	0.0609	-0.0003	-0.6553
		0	0.4675	0.0003	34.70
5415	C26	0	0.0767	-0.0001	-0.1113
		0	34.29	0.0004	34.62
5416	C25	0	0.0522	-0.0004	-0.0316
		0	0.0247	0.0007	34.66
5417	C18	0	0.2112	-0.0004	0.6942
		0	0.1916	0.0006	34.70
5418	C29	0	0.1560	-0.0002	1.139
		0	3.313	0.0002	34.70
5419	C30	0	0.0590	-0.0001	0.7103
		0	0.1367	0.0001	34.71
5421	C31	0	0.0138	-0.0002	1.090
		0	0.0528	0.0008	34.69
5423	C33	0	0.0197	-0.0003	0.6664
		0	0.0629	0.0006	34.71
-	C34			No CTD data at this station	
5426	C24	0	0.0652	-0.0005	1.096
		0	0.1012	0.0006	34.69
5427	C35	0	0.0183	-0.00045	0.5348
		0	0.0291	0	34.70

Table 6 summarises the MOCNESS and DTIS/Trawl station proximity, depth resolution and deepest sample depth for each of the core stations. In addition, the ETOPO1 (1 minute spatial resolution) bathymetric depth at each station location is reported (values in the three right-hand columns, italicized in braces). Note that only the CTD was deployed at the AE and ICOMM stations – no DTIS, trawl or MOCNESS deployments were conducted within 100 km of these stations. In Table 5, the closest matching MOCNESS or DTIS/Trawl station to the core station is highlighted. At station C25, the DTIS deployment was closer to the core station location (7 km compared to 11 km for the

MOCNESS), but the MOCNESS depth resolution was better, and both alternative deployments sampled depths similar to those found at the core station.

Table 6: Depth resolution of temperature and salinity upcast profiles from the Microcat units deployed with the MOCNESS and DTIS/trawl instruments. Note the variation in depths sampled by the three instruments, owing partly to differing sample location, partly to the objectives of each deployment and partly to data quality controls. The closest MOCNESS / DTIS station to each core station is highlighted in bold-face. Red highlighting denotes stations for which neither MOCNESS nor DTIS was deployed within 20 km of the core station location.

Station Name	Closest MOCNESS Station No. (and Distance from top of upcast to Core Station, km)	MOCNESS Microcat Depth resolution (m)	Closest DTIS Station No. (and Distance from Core Station, km)	DTIS Microcat Depth Resolution (m)	Deepest depth sampled [ETOPO 1' depth] (m)		
					CTD	MOC	DTIS
C1	42 (353 km)	1.0 ± 0.3	**26 (26 km)**	**2.2 ± 4.1**	272 [267]	717 [777]	219 [543]
C2	**42 (15 km)**	**1.0 ± 0.3**	66 (71 km)	2.2 ± 4.1	- [848]	717 [777]	400 [433]
C3	**57 (1.2 km)**	**0.9 ± 0.3**	56 (28 km)	9.7 ± 4.5	- [510]	478 [526]	484 [376]
C4	**95 (15 km)**	**0.3 ± 0.5**	94 (10 km)	8.4 ± 4.7	- [447]	398 [442]	400 [469]
C15	**122 (33 km)**	**1.1 ± 0.5**	115 (28km)	7.6 ± 4.1	451 [570]	791 [800]	427 [554]
C16	**122 (0.6 km)**	**1.1 ± 0.5**	115 (12km)	7.6 ± 4.1	- [858]	791 [800]	427 [554]
C17	**134 (23 km)**	**1.0 ± 0.4**	133 (12km)	12.7 ± 4.7	- [1531]	1696 [1572]	1522 [1504]
C27	**156 (10 km)**	**0.6 ± 0.5**	151 (19km)	6.8 ± 4.5	1661 [1476]	747 [834]	913 [530]
C26	**156 (16 km)**	**0.6 ± 0.5**	151 (9 km)	6.8 ± 4.5	841 [834]	747 [834]	913 [530]
C25	158 (18 km)	0.2 ± 0.3	151 (7 km)	6.8 ± 4.5	496 [515]	586 [704]	913 [530]
C18	**170 (24 km)**	**0.9 ± 0.3**	167 (45km)	9.9 ± 4.8	2156 [2209]	2098 [2210]	1880 [2117]
C29	**194 (152 km)**	**0.7 ± 0.2**	**183 (22km)**	**13.9 ± 4.6**	**1020** [695]	**533** [943]	**327** [3128]
C30	**194 (113 km)**	**0.7 ± 0.2**	**183 (80km)**	**13.9 ± 4.6**	**3213** [3280]	**533** [943]	**327** [3128]
C31	**194 (4.7 km)**	**0.7 ± 0.2**	198 (63km)	10.2 ± 1.3	601 [995]	533 [943]	632 [2987]
C33	**232 (44 km)**	**0.8 ± 0.4**	219 (73km)	12.5 ± 1.3	3367 [3566]	3303 [3566]	1169 [3574]
C34	**238 (4.8 km)**	**0.4 ± 0.3**	248 (29km)	10.8 ± 0.6	- [448]	174 [448]	704 [3601]
C24	**261 (4.3 km)**	**0.2 ± 0.2**	278 (7 km)	9.0 ± 2.6	438 [401]	397 [416]	736 [458]
C35	**283 (29 km)**	**0.8 ± 0.3**	278 (31km)	9.0 ± 2.6	3354 [3371]	3122 [3397]	736 [458]

Table 7: Differences in temperature (upper) and salinity (red, lower) between the second pair of CTD stations and the MOCNESS Microcat.

CTD station	Station Name	Temperature [Salinity] difference statistics					Median T [S] in profile
		Min	Max	Median	Median %	Std dev. %	
n/a	AE1	No MOCNESS data within 100 km of these stations					
u5402	ICOMM55	No MOCNESS data within 100 km of these stations					
u5403	ICOMM60	No MOCNESS data within 100 km of these stations					
u5404	AE2	No MOCNESS data within 100 km of these stations					
u5405	ICOMM65	No MOCNESS data within 100 km of these stations					
5406	C1	00162	0.7359	0.0370	1.96	28.4	-1.876
		0.0055	0.3962	0.0205	0.058	0.253	34.65
-	C2	No CTD data at these stations					
-	C3	No CTD data at these stations					
-	C4	No CTD data at these stations					
5411	C15	0.0119	1.776	0.3018	129	96.0	-1.021
		0.0004	0.3188	0.0756	0.223	0.158	34.48
-	C16	No CTD data at these stations					
-	C17	No CTD data at these stations					
5414	C27	1.551	1.647	1.593	191	0.940	0.657
		0.0921	0.1061	0.0967	0.279	0.012	34.71
5415	C26	0.2313	0.6742	0.5779	324	171	-0.109
		0.0445	0.0571	0.0479	0.138	0.011	34.63
5416	C25	0.0047	1.857	0.2212	53.4	922	-0.029
		0.0003	0.1395	0.0399	0.115	0.100	34.67
5417	C18	2.9e-5	1.299	0.0150	2.08	322	0.696
		0.0282	0.1732	0.0434	0.125	0.071	34.71
5418	C29	0.0005	1.115	0.0978	8.31	122	1.139
		0.0063	0.4087	0.0511	0.148	0.217	34.70
5419	C30	0.0027	0.5297	0.2214	16.5	128	0.712
		0.0006	0.4002	0.0566	0.163	0.158	34.71
5421	C31	0.0023	0.7257	0.1047	9.02	212	1.090
		0.0007	0.3286	0.0443	0.128	0.143	34.70
5423	C33	0.0003	0.6934	0.0302	4.34	50.4	0.668
		0.0002	0.1254	0.0444	0.128	0.025	34.71
-	C34	No CTD data at this station					
5426	C24	0.0008	0.3237	0.0489	4.26	40.9	1.097
		0.0009	0.1194	0.0439	0.127	0.047	34.70
5427	C35	5.00e-5	0.3827	0.0228	3.51	86.2	0.535
		0.0019	0.0958	0.0446	0.129	0.022	34.71

Table 8: Differences in temperature (upper) and salinity (red, lower) between the second pair of CTD sensors and the DTIS/Trawl Microcat.

CTD station	Station Name	Temperature [Salinity] difference statistics					Median T [S] in profile
		Min	Max	Median	Median %	Std dev. %	
n/a	AE1	No DTIS data within 100 km of these stations					
u5402	ICOMM55	No DTIS data within 100 km of these stations					
u5403	ICOMM60	No DTIS data within 100 km of these stations					
u5404	AE2	No DTIS data within 100 km of these stations					
u5405	ICOMM65	No DTIS data within 100 km of these stations					
5406	C1	1.07e-6	0.2908	0.0058	0.301	6.54	-1.876
		9.25e-5	0.4375	0.064	0.018	0.160	34.65
-	C2	No CTD data at these stations					
-	C3	No CTD data at these stations					
-	C4	No CTD data at these stations					
5411	C15	0.0001	0.7509	0.1410	25.5	139	-1.021
		1.25e-4	0.3830	0.0265	0.077	0.210	34.48
-	C16	No CTD data at these stations					
-	C17	No CTD data at these stations					
5414	C27	0.0088	1.636	0.8510	92.2	380	0.657
		0.0306	0.3277	0.0738	0.213	0.251	34.71
5415	C26	0.0006	0.7876	0.2545	110	223	-0.109
		4.34e-5	0.2841	0.0226	0.065	0.081	34.63
5416	C25	0.0078	2.483	0.4266	114	2171	-0.029
		6.02e-4	0.1588	0.0637	0.184	0.126	34.67
5417	C18	0.0254	1.0055	0.1367	20.1	135	0.696
		0.0010	0.1988	0.0095	0.027	0.085	34.71
5418	C29	3.12e-5	0.9723	0.1532	12.9	70.4	1.139
		0.0003	0.5507	0.0503	0.145	0.511	34.70
5419	C30	0.0013	1.5074	0.2358	16.0	934	0.712
		0.0001	0.5001	0.0611	0.177	0.308	34.71
5421	C31	0.0008	0.5210	0.0574	4.47	167	1.090
		7.44e-5	0.0946	0.0452	0.130	0.052	34.70
5423	C33	0.0033	1.5461	0.1682	12.3	120	0.668
		9.18e-5	0.2878	0.0467	0.135	0.101	34.71
-	C34	No CTD data at this station					
5426	C24	0.0046	0.4150	0.0582	5.27	155	1.097
		0.0058	0.1950	0.0315	0.091	0.092	34.70
5427	C35	0.0002	0.2809	0.1130	9.09	53.3	0.535
		0.0009	0.2063	0.0288	0.083	0.088	34.71

Table 9: Differences in temperature (upper) and salinity (red, lower) between the DTIS/Trawl Microcat and the MOCNESS Microcat.

CTD station	Station Name	Temperature [Salinity] difference statistics					Median T [S] in profile
		Min	Max	Median	Median %	Std dev. %	
n/a	AE1	No DTIS or MOCNESS data within 100 km of these stations					
u5402	ICOMM55	No DTIS or MOCNESS data within 100 km of these stations					
u5403	ICOMM60	No DTIS or MOCNESS data within 100 km of these stations					
u5404	AE2	No DTIS or MOCNESS data within 100 km of these stations					
u5405	ICOMM65	No DTIS or MOCNESS data within 100 km of these stations					
5406	C1	0.00932	0.6184	0.0368	1.92	13.0	-1.93
		0.0068	0.4321	0.0252	0.073	0.341	34.72
-	C2	4.05e-5	0.4463	0.0317	1.64	6.77	-1.93
		0.0154	0.7015	0.0269	0.078	0.394	34.72
-	C3	0.0016	0.8061	0.0320	1.70	11.8	-1.89
		3.07e-5	0.0784	0.0294	0.085	0.045	34.61
-	C4	0.0016	0.1547	0.0432	2.69	2.02	-1.74
		0.0043	0.0365	0.0264	0.077	0.021	34.44
5411	C15	0.0144	1.603	0.4609	79.2	561	-0.397
		0.0512	0.2385	0.1163	0.339	0.127	34.59
-	C16	0.0144	1.603	0.4609	79.3	561	-0.40
		0.0512	0.2385	0.1163	0.339	0.127	34.59
-	C17	2.52e-5	0.3083	0.0191	2.27	63.9	0.755
		14.4	15.5	15.5	80.4	1.66	34.59
5414	C27	0.0342	0.1956	0.0905	12.0	7.09	-0.759
		0.0239	0.0323	0.0264	0.076	0.006	34.62
5415	C26	0.0342	0.1956	0.0905	12.0	7.09	-0.759
		0.0239	0.0323	0.0264	0.076	0.006	34.62
5416	C25	0.0003	1.173	0.4066	117	2114	-0.074
		0.0010	0.1176	0.0510	0.147	0.088	34.61
5417	C18	0.0067	0.6949	0.1329	20.3	170	0.683
		4.98e-5	0.2042	0.0344	0.099	0.094	34.67
5418	C29	3.78e-5	1.371	0.4185	37.7	537	1.073
		0.0298	0.2095	0.1153	0.337	0.177	34.62
5419	C30	No DTIS or MOCNESS stations within 60 km					
5421	C31	0.0024	0.3013	0.0856	7.16	61.4	1.073
		0.0002	0.3989	0.0100	0.027	0.168	34.62
5423	C33	0.0039	1.489	0.1298	10.0	146	0.656
		4.27e-5	0.2378	0.0095	0.027	0.116	34.67
-	C34	0.0051	0.8004	0.0588	7.94	763	0.616
		0.0005	0.3489	0.0206	0.059	0.275	34.52
5426	C24	0.0030	0.3510	0.0992	9.62	968	0.985
		0.0002	0.1879	0.0138	0.040	0.092	34.62
5427	C35	0.0003	0.2296	0.0965	7.90	36.9	0.563
		0.0002	0.1376	0.0125	0.036	0.061	34.66

2. RESULTS

2.1 Objective 4A

In vitro fluorometric and HPLC chlorophyll-a measurements were compared to assess data quality. Discrete chlorophyll samples were analysed in four different subsets according to the sampling objectives of different research groups, and these subsets were generally in good agreement (Figure 3). A positive bias was found between in vitro fluorometric measurements and the HPLC dataset, as expected (e.g. Welschmeyer, 1994). The bias ranged from 1.2 to 1.6. The strongest correlation was found between HPLC and the Objective 4 in vitro fluorometric chl-a data. Since the latter dataset was the largest (N = 61), the subset of HPLC-fluorometric Chl-a matched data pairs were used to correct the in vitro fluorometric values. The correction equation to normalise in vitro fluorometric (measured in the NIWA Hamilton laboratory) to HPLC-equivalent chlorophyll-a values is:

HPLC-equivalent chl-a = in vitro fluorometric chl-a × 0.5224[± 0.0343] + 0.0364[± 0.0181]
(r^2 = 0.50, n = 42, p = 0.05).

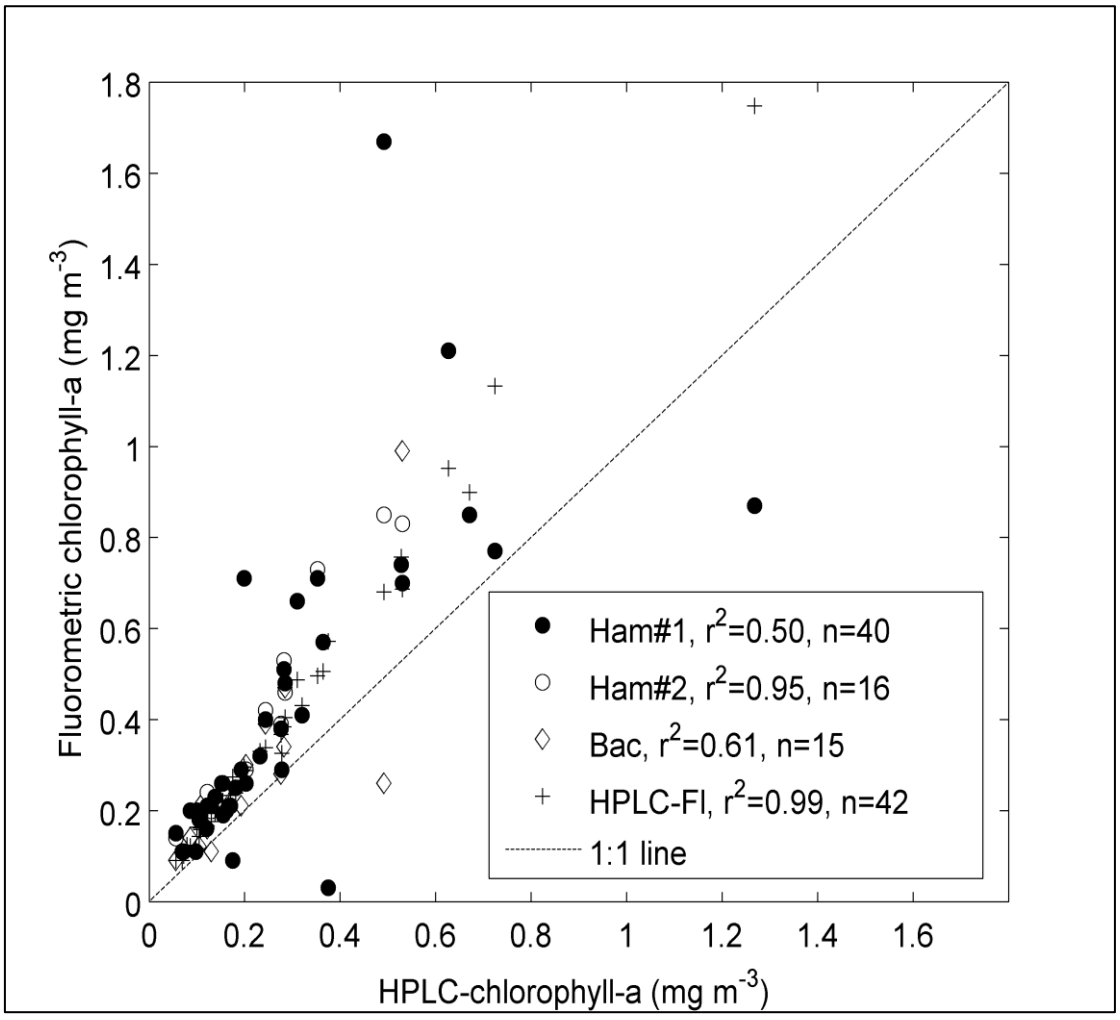

Figure 3: Comparison of multiple in situ chlorophyll-a datasets.

With confidence in the chl-a measurements, the underway Turner fluorometer (in vivo fluorescence) was calibrated against in situ measurements by extracting 1 minute of despiked fluorometer values over the water sampling period. The despiked beam attenuation measurements were likewise calibrated against in situ POC measurements. Calibration of beam attenuation against POC was

complicated because of a few sparsely sampled stations with very high attenuation efficiency – these are represented by the cloud of measurements below the calibration line in Figure 4. No systematic relationship was found between these points and latitude, longitude, depth or chlorophyll. The final calibrated POC profiles derived using this calibration are therefore an underestimate of likely POC concentrations at some stations. The agreement between the two underway chlorophyll in vivo fluorometers (Turner and Wetlabs-Ecotriplet) was $r^2 = 0.6912$. These calibrations were applied to the CTD and underway data to provide high depth- and spatial-resolution information. The calibrations are shown in Figures 4 and 5, and the equations are:

CTD profiling sensor calibrations:

Conversion between HPLC and in vivo fluorometric chlorophyll-a:
Flu-Chl-a = 1.22[± 0.07] × HPLC-chla + 0.05[±0.02]; ($r^2 = 0.50$, n = 40)

CTD chl-a = in vivo fluorescence × 0.0737 [± 0.0064]; ($r^2 = 0.25$, n = 61)

The POC calibration is given firstly for the entire dataset, and then for subsets of the data, based on chlorophyll-a concentration and on latitude (see Figure 5).

CTD POC = beam attenuation × 156.28 [±16.73];
($r^2 = 0.266$, n = 130, $p << 0.1$)

CTD POC (South of 70°S) = beam attenuation × 564.87[± 53.12] + 19.25[± 3.93];
(bold dashed line in Figure 4B) ($r^2 = 0.67$, n = 57, $p << 0.1$)

CTD POC (North of 70°S, chl ≥ 0.4) = beam attenuation × 412.58[± 256.51] + 41.63[± 55.87];
($r^2 = 0.51$, n = 5, p = 0.5)

CTD POC (North of 70°S, chl < 0.4) = beam attenuation × 44.84[± 24.76] + 36.77[± 9.56];
(thin dashed line in Figure 4B) ($r^2 = 0.14$, n = 28, $p < 0.1$)

Underway sensor calibrations:

Underway chl-a = fluorescence 0.0908[±0.0156] – 0.3438[±0.1127]; ($r^2 = 0.53$, n = 28, p = 0.0052)

Underway POC = beam attenuation ×456.52[± 22.94]; ($r^2 = 0.80$, n = 18, $p << 0.1$)

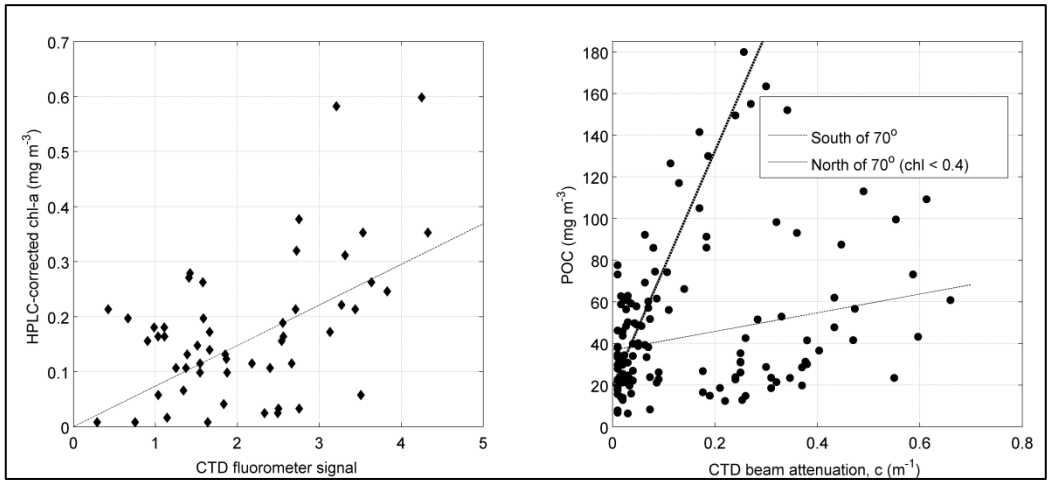

Figure 4: Calibration of the CTD fluorescence and beam attenuation data against matched lab samples.

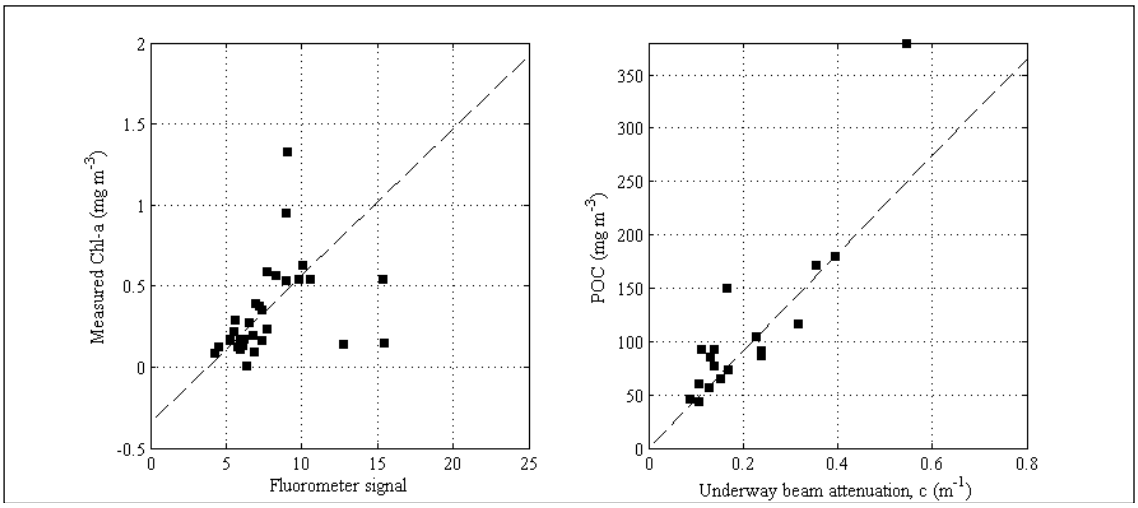

Figure 5: Calibration of the CTD-profiled fluorescence and beam attenuation data against matched lab samples.

Calibrated in vivo fluorometer and transmissometer data were used to produce maps of surface chlorophyll-a and POC concentrations (Figure 6). Two patches were sampled in which both POC and chlorophyll-a were elevated, with values exceeding 0.5 mg m^{-3} chlorophyll-a and 400 mg m^{-3} POC. These values can be compared against satellite-derived surface chlorophyll-a and POC values as an empirical validation of the (global) NASA algorithms for these waters.

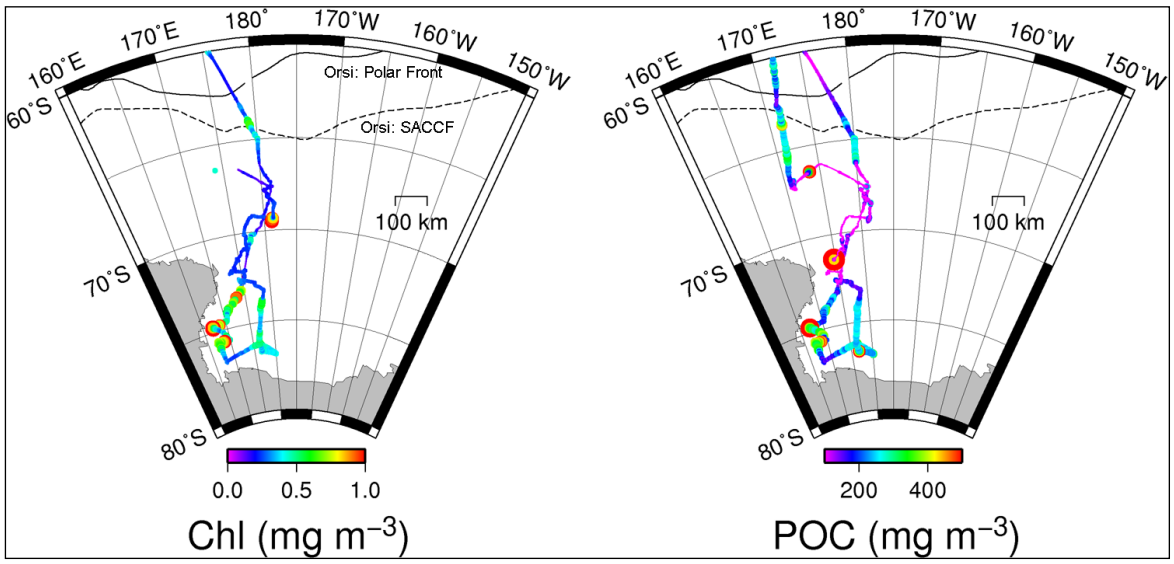

Figure 6: Mapped surface chlorophyll-a and POC derived by calibrating the underway fluorometer and transmissometer.

POC and chlorophyll distributions were closely coupled for much of the survey, with the exception of high chlorophyll-low POC waters at approximately 69 °S, and a slight north-south disjoint at the Southern ACC front (SACCF), with high chlorophyll located slightly northwards of the POC peak on the southward journey. Variation in the POC:Chl-a ratio indicates either a change in the microbial community composition (species change) or an adaptation of the community (with no species change) to changing light and/or nutrient environments. Chang et al. (2012) report subtle variations in relative abundance of pennate diatoms, small-celled diatoms, Phaeocystis spp. and dinoflagellates along

north-south gradients. Of 74 species recorded, 39 were present in all water masses. The two numerically most abundant species (*Fragilariopsis kerguelensis* and *Phaeocystis antarctica*) on the shelf were less abundant off the shelf and in open waters no other species replaced their high numbers. This could suggest that adaptation was the main factor affecting POC:Chl-a ratios, but a shift from a bi-specific to a more mixed community also contributed. The dataset acquired is not sufficient to deconvolve the bio-optical variability observed (no statistical significance was found). A full report of microbial variability is given in Stephens et al., (2010) and Chang et al. (2012).

Optical backscatter data from the Wetlabs VSF3 can be compared directly against satellite-derived backscatter values. Attempts to fit a full volume scattering coefficient (i.e. scattering at each degree from 0° (forwards scattering), to 180° (backwards scattering)) were not successful, but a cursory analysis of backward and sideward scatter (Figure 7) shows spatial variability in each of these parameters and facilitates comparison between scattering and the concentrations of chlorophyll and POC. The scattering signals were well-correlated with one another for the majority of the voyage, and agreed well with chlorophyll and POC distributions for the majority of the voyage. However, of particular note is the absence of elevated sidewards scatter in the phytoplankton bloom at the northern edge of the Ross Sea. Given the large uncertainty in the fluorometer calibration, it cannot be ruled out that this discrepancy is caused by variability in the chlorophyll-specific fluorescence. There are also known problems with the VSF3 measurement chamber, for which stray light characterisation is difficult. If the scattering data quality can be assured using inherent optical property consistency checks, then the ratio of VSF3-measured backscatter to particulate organic carbon can also be used to evaluate carbon-based primary production algorithms (Behrenfeld et al. 2005).

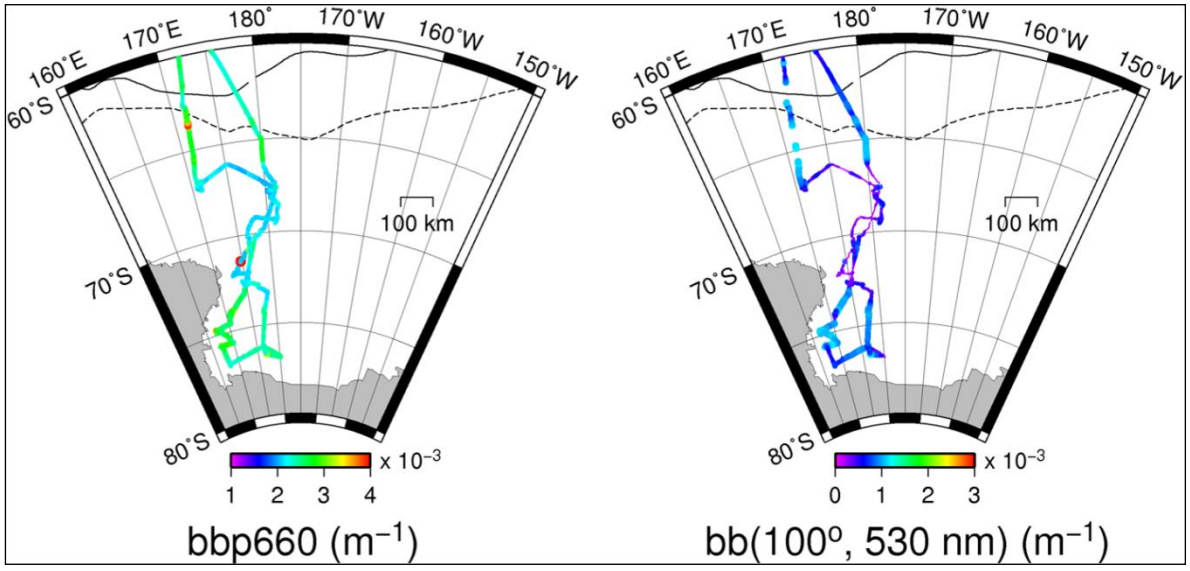

Figure 7: Backscattering in the red and sidewards scattering in the green, measured by the underway Wetlabs VSF3.

Ideally, the Wetlabs-Ecotriplet CDOM fluorometer would be calibrated against spectrophotometrically measured CDOM absorption. This comparison would quantify the degree of spatial consistency of fluorescence efficiency, providing an indication of changes in CDOM composition. However, concentrations of CDOM tend to be very low in the Southern Ocean, and the spectrophotometric signal measured from filtered samples on the IPY-CAML voyage was too close to the instrument detection limits for the CDOM fluorometer to be calibrated. The CDOM fluorometry data remain in arbitrary units and are shown in Figure 8. Although the signal range was very small (0.21 to 0.39 arbitrary units across the entire survey region), indicating that this sensor is not particularly sensitive, a marked south-north gradient was detected, with maximum values occurring toward the south-centre of the Ross Sea. We conclude that either the concentrations of fluorescent material were higher in the south, or that fluorescence efficiency was higher in the south. The absence

of continued signal elevation during the homeward voyage transect indicates that no significant bio-fouling occurred in the underway system. Weakly elevated CDOM fluorescence values were also observed in the location of peak chlorophyll-a and POC at the west side of the Ross Sea. Elevated CDOM concentrations might be associated with the sympagic ice-alga community, with healthy phytoplankton communities or with senescent blooms. Since only healthy phytoplankton cells were identified in the taxonomy work undertaken in Objective 3, and because the filter papers used for measuring absorption could not be bleached to yield a 'detrital' absorption component for comparison with CDOM results (in order that HPLC analysis could be carried out on the same filter papers), we were not able to infer CDOM sources from this dataset.

CDOM fluorescence data from the Wetlabs Ecotriplet cannot be compared directly with satellite products because the signal received by ocean colour satellite radiometers depends on the combined optical effect of all coloured material in the water as well as the incident light field. Although CDOM absorption can be inferred using algorithms, the fluorescence efficiency of CDOM is known to vary with the composition of the dissolved substances (Kowalczuk et al. 2005). CDOM can not yet be chemically characterised using any known laboratory procedure, although dissolved organic carbon is often derived using CDOM absorption measurements with a frequent standard calibration.

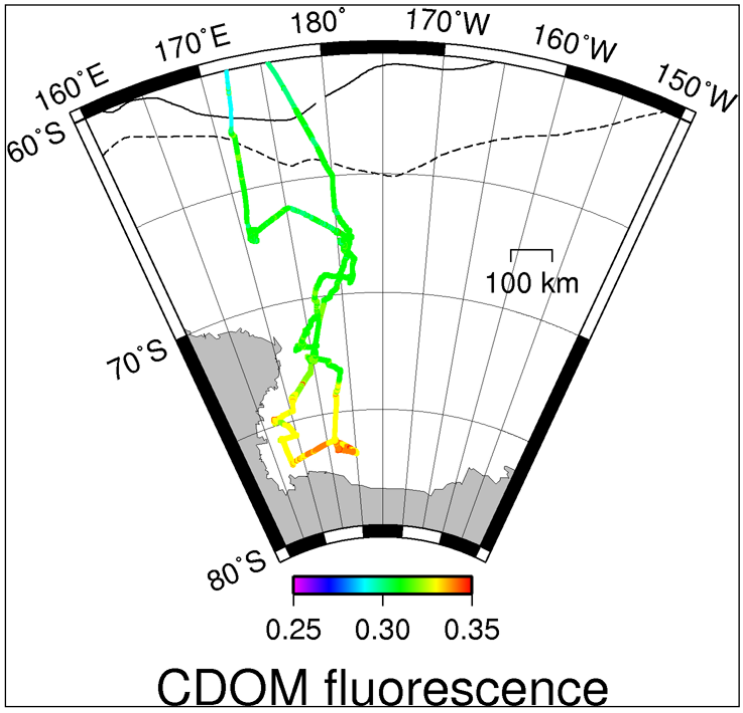

Figure 8: CDOM fluorescence measured by the underway Wetlabs Ecotriplet.

MODIS-Aqua ocean colour imagery

During the IPY voyage, 898 5-minute granules of data from the Moderate Resolution Imaging Spectrometer (MODIS-Aqua), operated by NASA, were recorded covering some area of the Ross Sea. Of these images, 583 granules contained some (more than 1%) ice- and cloud-free pixels. However, few temporal match-ups with the exact ship location were obtained owing to cloud cover. A comparison between satellite-derived and in situ-measured parameter frequency distributions is the most useful quantitative validation exercise possible with this dataset.

Figure 9 shows true-colour composites derived from MODIS for one day. Between 03:25 and 03:30 UTC, ice- and cloud-free coverage of the polar front, north of the Ross Sea, was obtained, but the preceding granule at 03:20 which would show the Ross Sea itself was 100% cloudy. The later overpass at 05:05 UTC (Figure 9, lower panel) does include clear pixels in the western Ross Sea, however, at this time, the sun-angle is more oblique and the signal to noise ratio is higher. Analysis of the MODIS imagery and comparison with in situ data is ongoing (Schwarz et al., 2012).

AMSR-E sea ice data

The Advanced Microwave Scanning Radiometer operated by Jaxa for NASA provides an estimate of ice areal coverage using passive measurements of upwelling microwave radiation (Spreen et al. 2008). The nine-year AMSR-E dataset was analysed for the Ross Sea to give a medium-term average against which to compare the IPY voyage period. This provides a useful measure of how typical were conditions during the IPY voyage, since sea-ice concentrations are impacted by climatic conditions (Lovenduski & Gruber, 2005). Monthly sea-ice data were obtained from (http://www.ifm.zmaw.de/en/research/remote-sensing-assimilation/sea-ice/ University of Hamburg, Institute of Oceanography, Gunnar Spreen and Lars Kaleschke) and classified (after Smith et al. 2011) into five concentration classes of:

i.	0%	Ice-free water
ii.	1–15%	Open water with isolated sea-ice
iii.	16–40%	Marginal sea-ice
iv.	41–80%	Unconsolidated pack-ice
v.	80–100%	Consolidated pack-ice

Monthly ice concentrations were found to be exceptionally high during the voyage season, and persistence of the 80–100% ice class was longer than the 9-year (2003 to 2011) norm. Ice class anomalies for the voyage are shown in Figure 10.

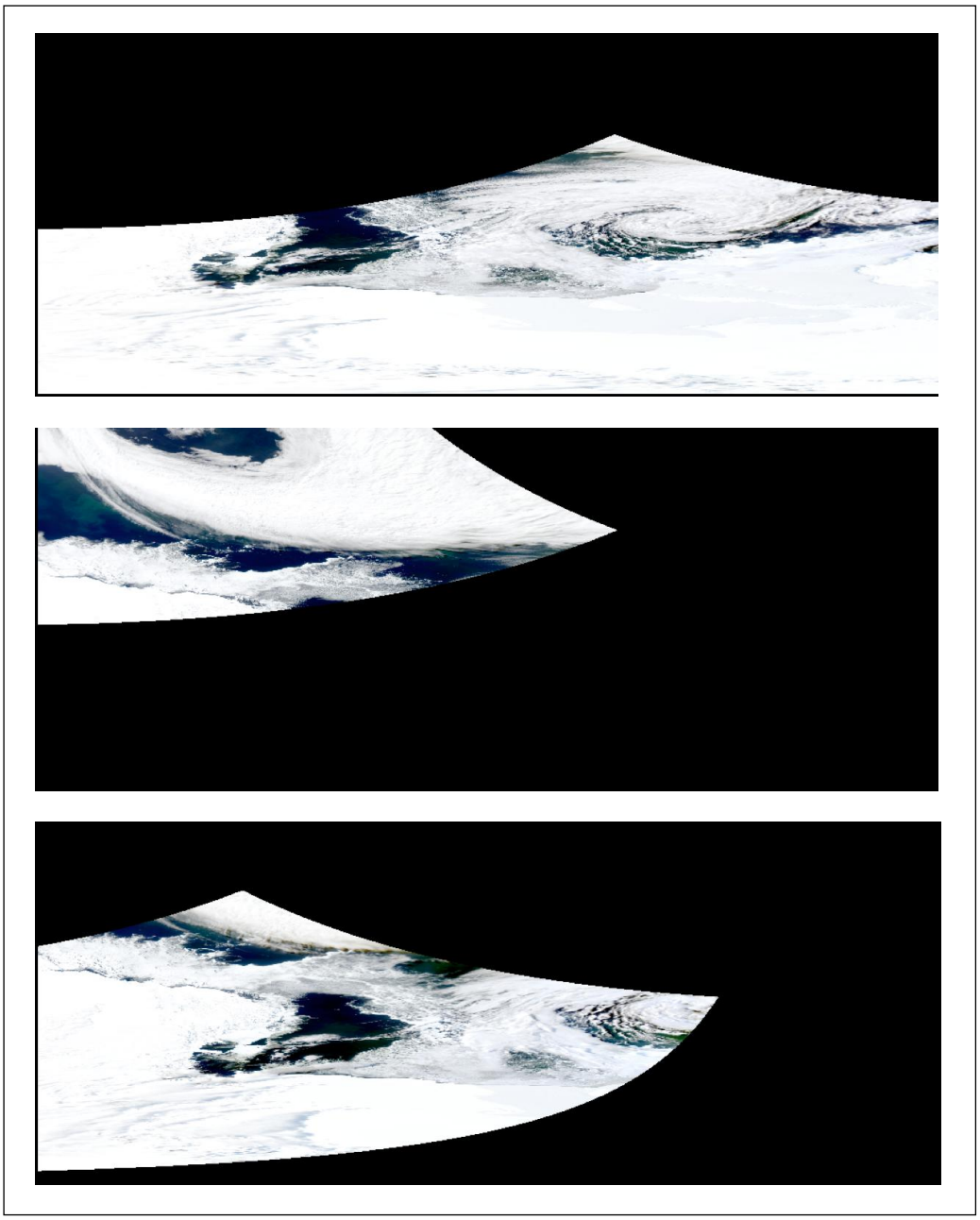

Figure 9: True colour composite images of the Ross Sea on Julian Day 55 (24 February) at 03:25, 03:30 and 05:05 UTC. Derived from MODIS data kindly provided by NASA, using SeaDAS v6.0.

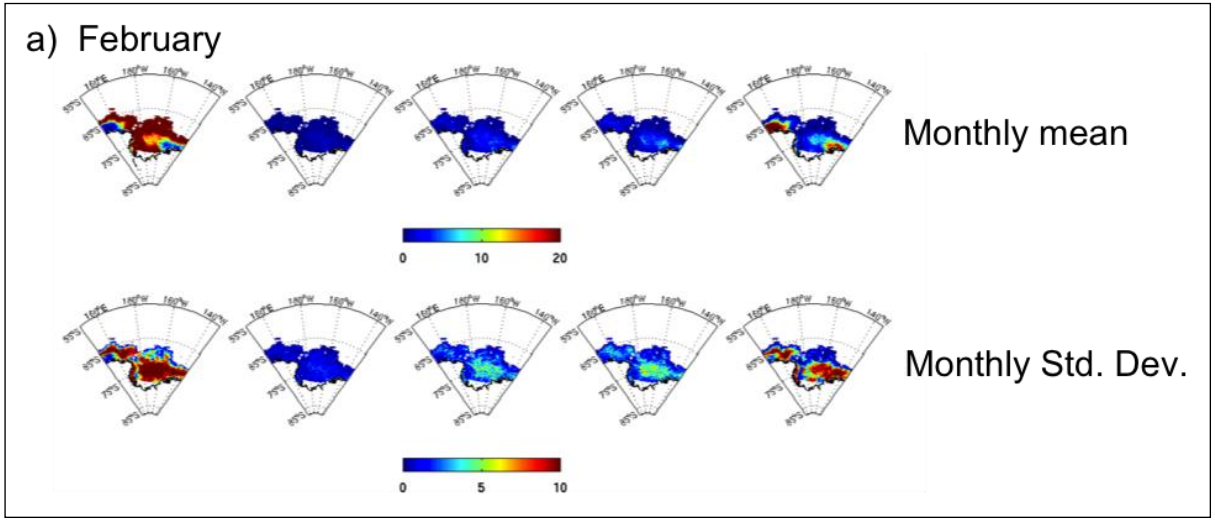

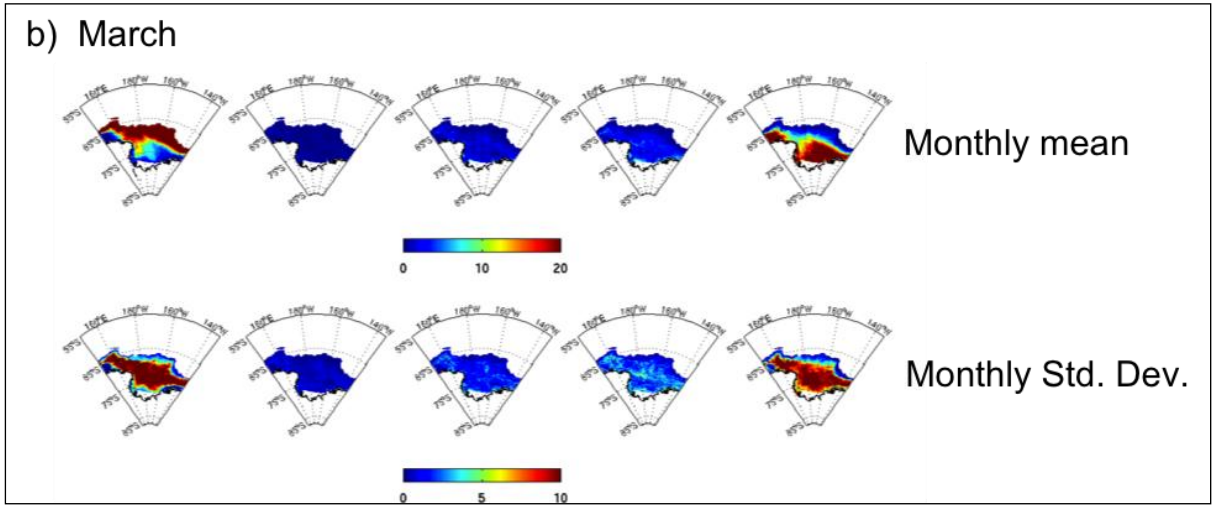

Figure 10: Mean monthly number of days for which each pixel is classified as belonging to ice classes 1 (left) to 5 (right), and the standard deviation, calculated using AMSR-E data for a) February and b) March, in each case from 2003 to 2011.

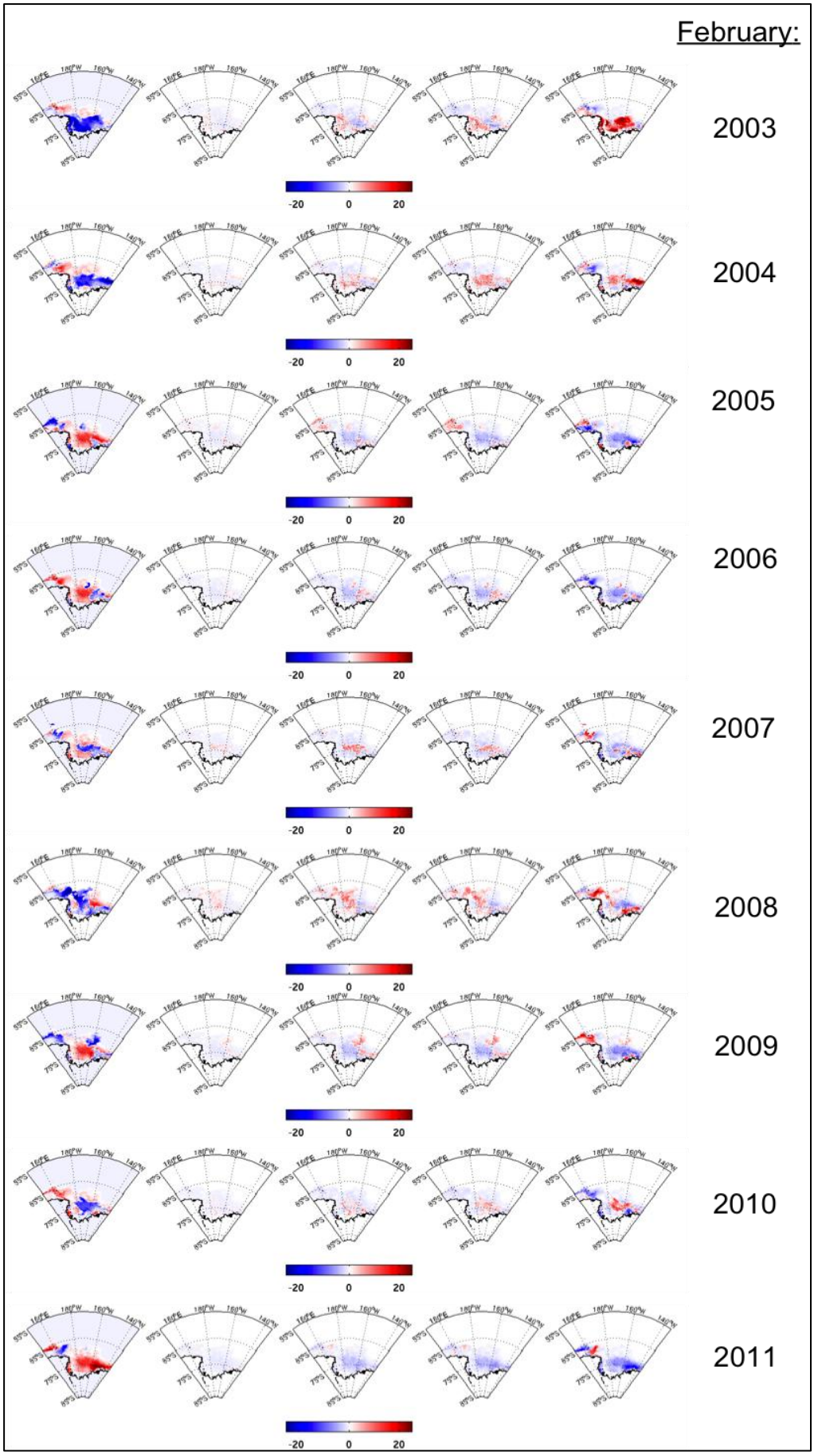

Figure 11: Sea ice class membership anomalies for February 2003 to 2011.

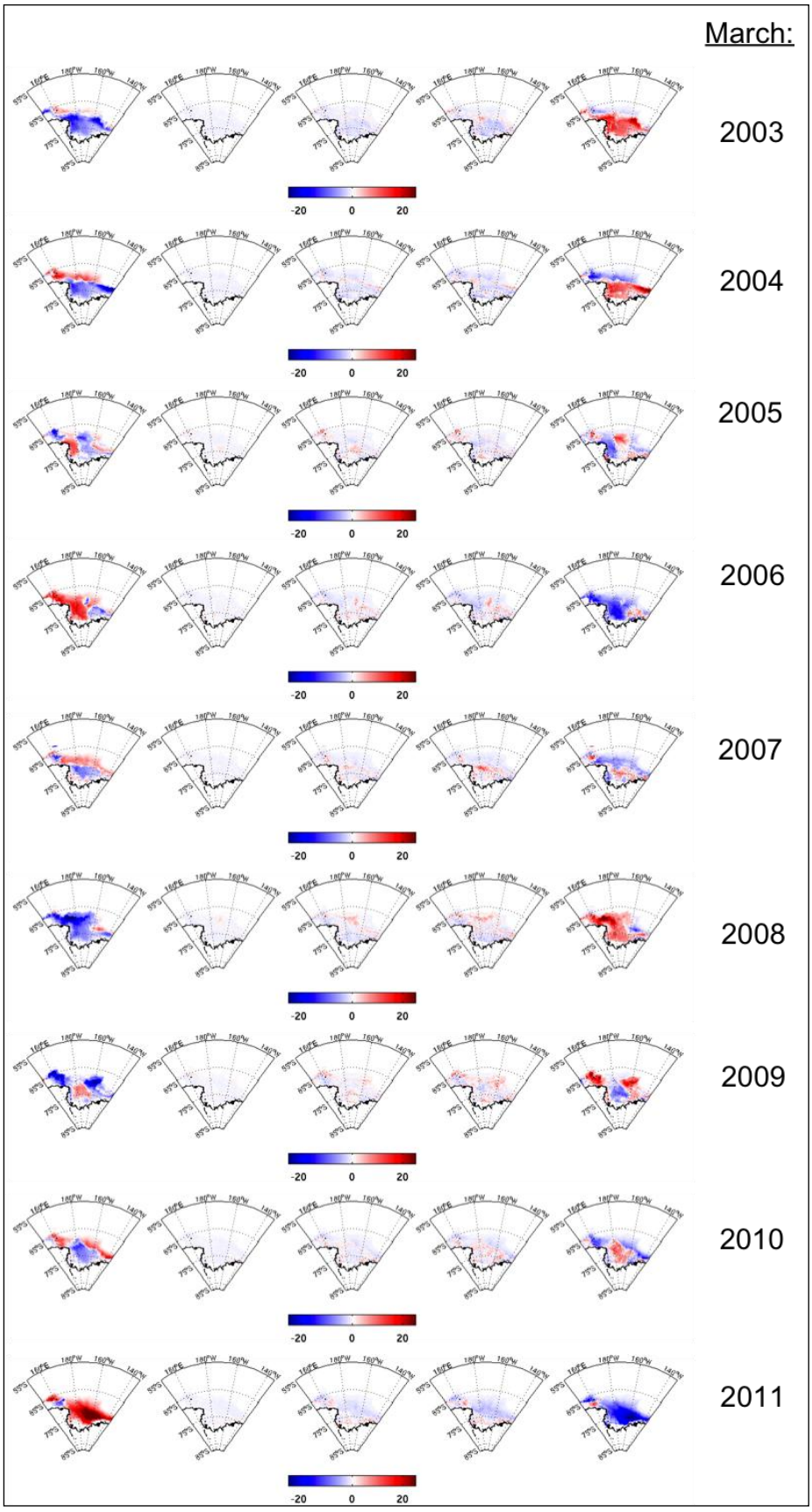

Figure 12: Sea ice class membership anomalies for March 2003 to 2011.

During the voyage season, membership of the 0% ice class was up to 20% lower than the 9-year mean across the western side of the Ross Sea, whilst membership of the 80 – 100% ice class was up to 20% higher than the 9-year mean (Figures 11, 12). Membership of the intermediate classes was within 5% of the mean. The spacial anomalies were patchier during February 2008 than March 2008. This suggests greater persistence of sea-ice during the voyage year than has been found in the past decade. Correlation of sea ice anomalies against the Southern Oscillation Index and Southern Annular Mode, both of which serve as measures of large-scale climatic pattern anomalies, yielded significant correlations with the SOI and lower signficance correlations with the SAM. This is consistent with other studies of sea ice variability in the Ross Sea (e.g. Stammerjohn et al. 2008), but note that the period of the analysis is short compared with known climatological oscillations. Correlations between sea ice anomalies, SOI and SAM indices are shown in Figure 13.

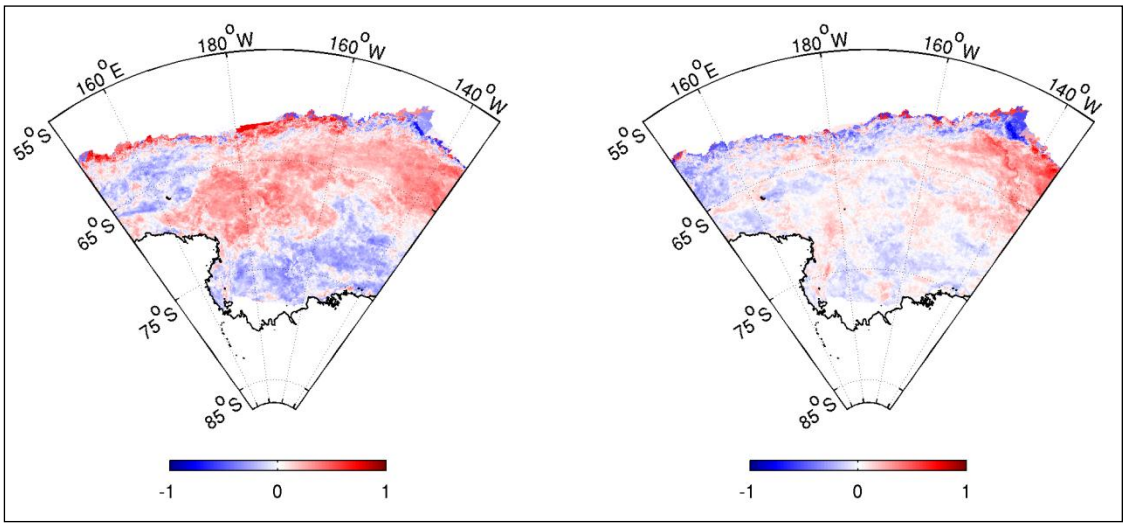

Figure 13: Correlation coefficient between sea-ice anomalies and (left) the Southern Oscillation Index and (right) the Southern Annular mode.

2.2 Objective 4B

Examples of the different temperature and salinity profiles obtained using CTD, DTIS and MOCNESS-mounted devices on the shelf, continental slope and in deep waters are shown in Figures 14 to 16. Figure 17 shows the spatial variability in temperature and salinity as measured using the underway system.

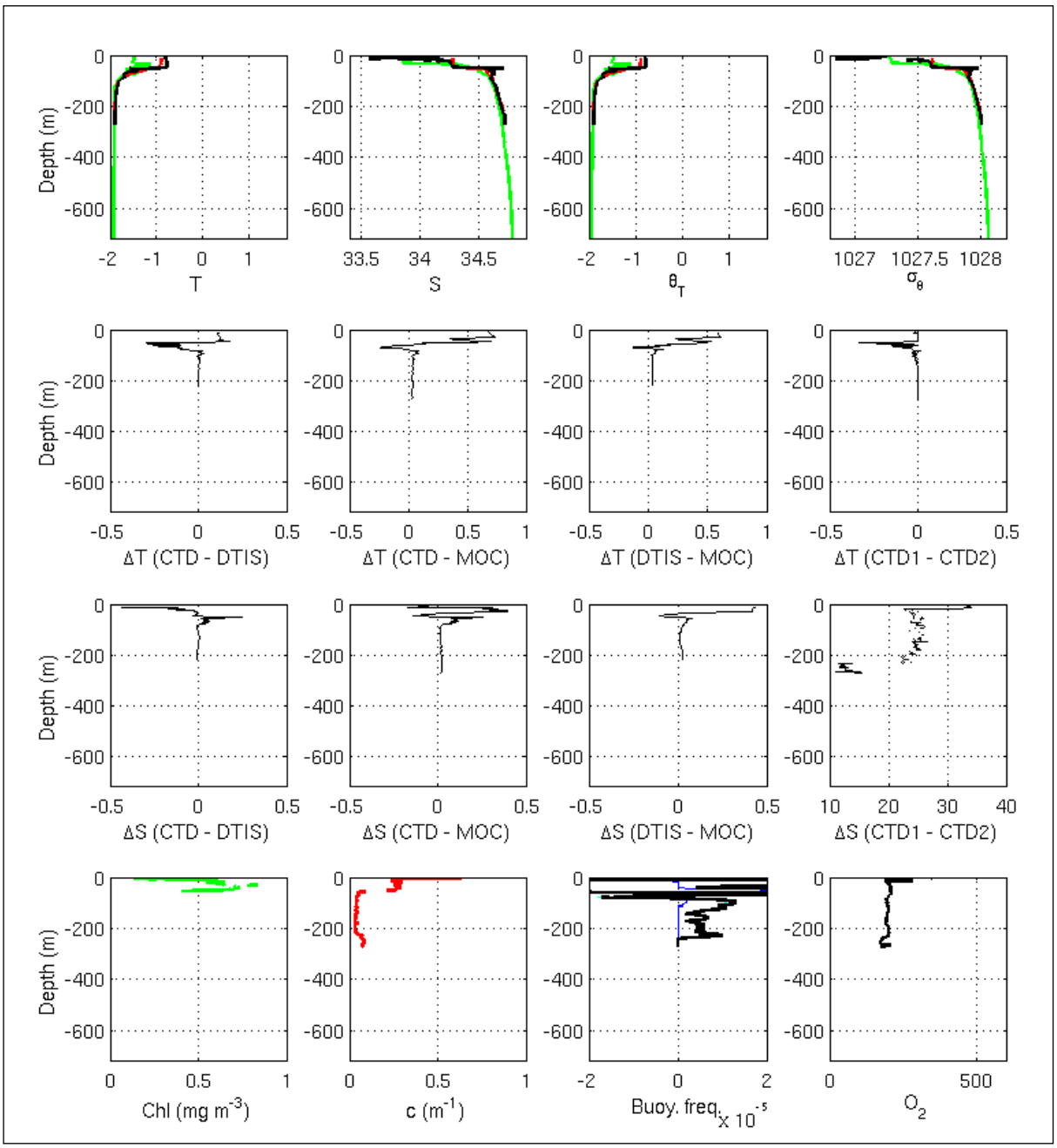

Figure 14: Temperature, salinity and derived parameters from the CTD, MOCNESS and DTIS deployments at core station C1, on the continental shelf.

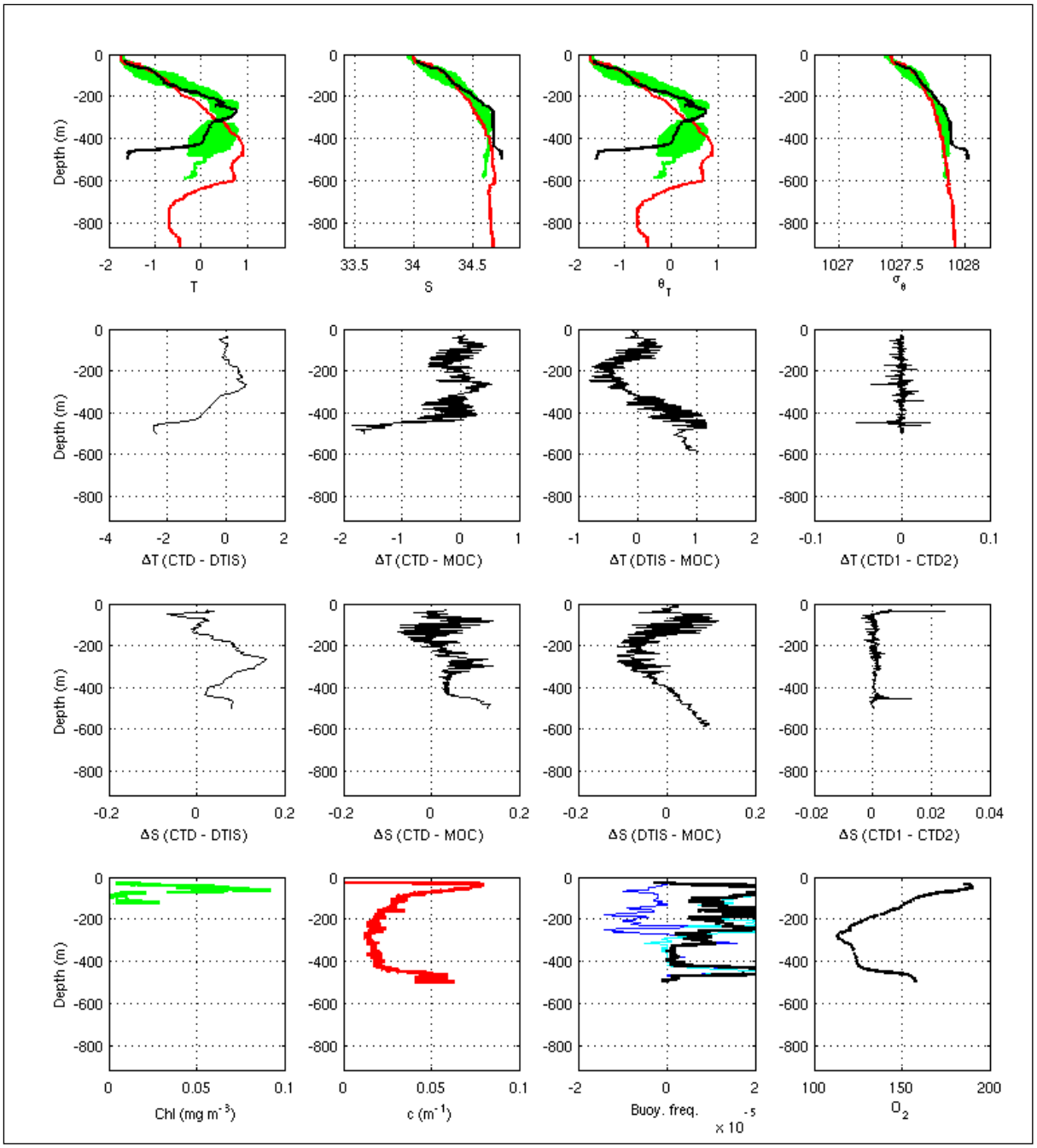

Figure 15: Temperature, salinity and derived parameters from the CTD, MOCNESS and DTIS deployments at core station C25, on the continental slope.

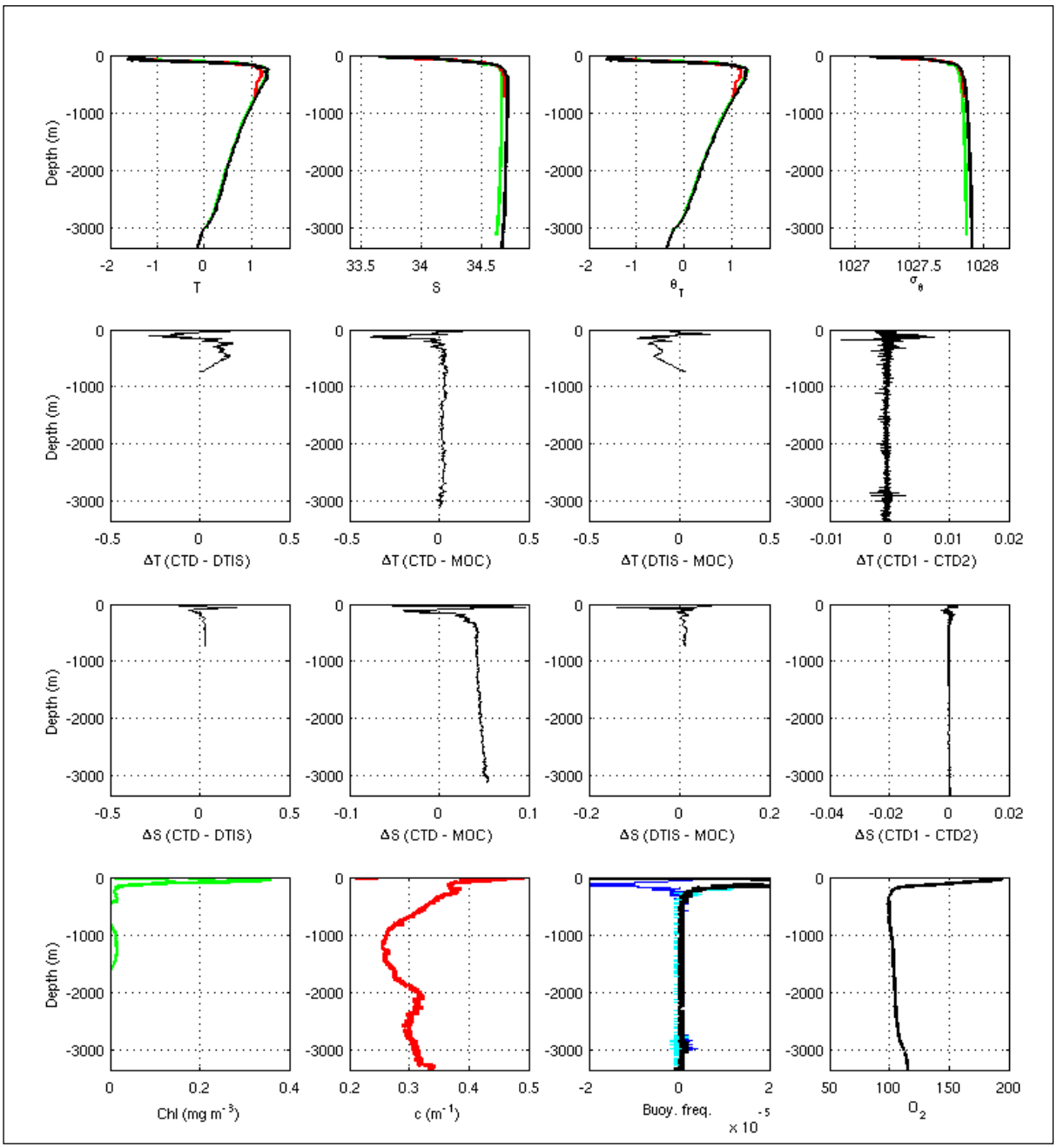

Figure 16: Temperature, salinity and derived parameters from the CTD, MOCNESS and DTIS deployments at core station C35, in the deep Southern Ocean.

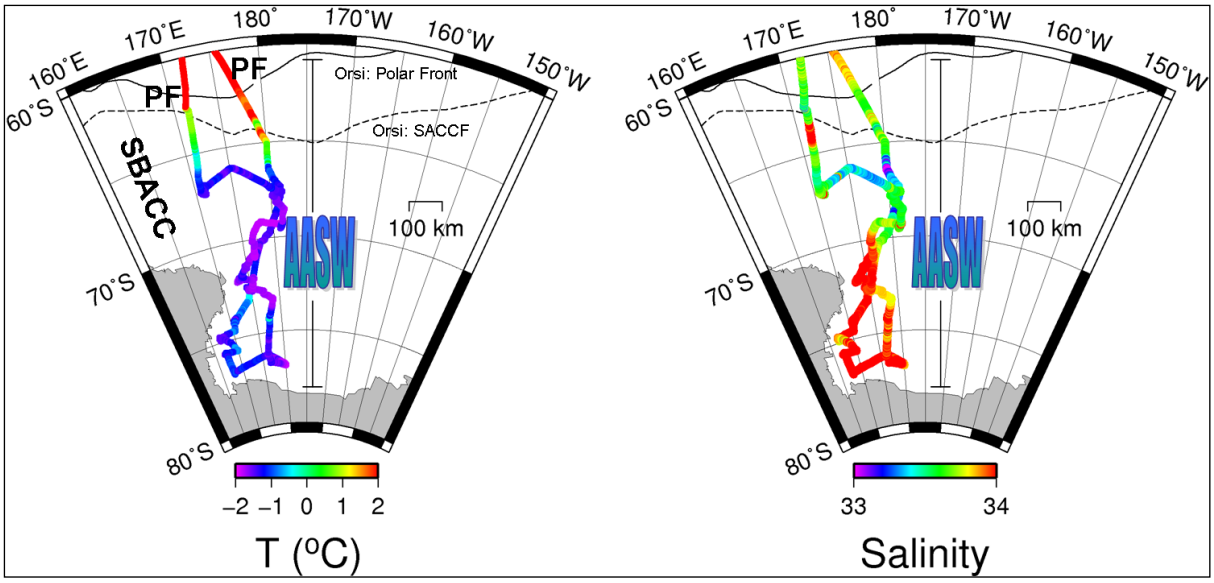

Figure 17: Surface temperature and salinity distributions as measured using the underway system. AASW: Antarctic Surface Water. Fronts are indicated according to Orsi et al. (1995).

The surface temperature, salinity and nutrient ranges of stations on the shelf, continental slope and in deep waters are summarised in Table 10. Nitrate concentrations were high at most locations north of 74°S, and were always above 40 mg m^{-3}, i.e. nitrate was never limiting. Ammonia concentrations were anomalously high at three stations: at about 73°S this coincided with lower NO_3^- and high POC (refer to Figure 6); at about 76°S the elevated NH_4^+ signal coincided with high chlorophyll and low NO_3^-; at the northernmost point, POC values were low and no underway chlorophyll data were available. The nitrogen:phosphate ratio was relatively constant throughout the region at 11.5 (mol:mol). Figure 18 shows the nitrate to phosphate ratios at all depths sampled, while Figure 19 shows the spatial distribution of surface nutrient concentrations. No depth gradients in nutrients or nutrient ratios were found. However, nutrient values were most depleted on the shelf, and the slope stations exhibited greatest variability. Because of the attachment of nitrate-containing chains with benzene molecules in the dissolved organic seawater fraction, some agreement might be expected between nutrient values and CDOM fluorescence (Schwarz et al. 2001). However, no consistent correlations between any of the nutrient concentrations and CDOM fluorescence were observed during the voyage. Instead, core station nutrient measurements were patchy (see Figures 8 and 19).

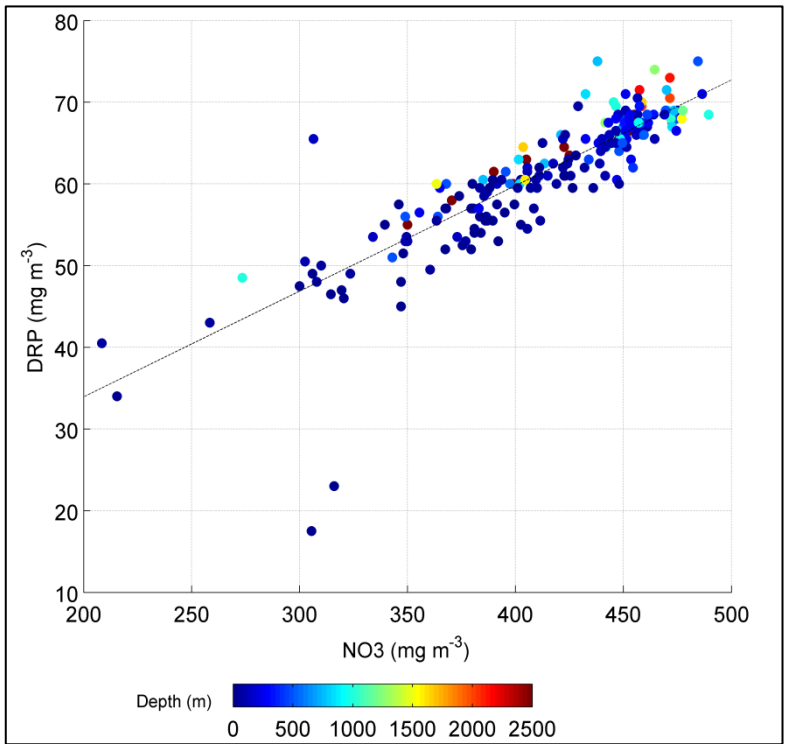

Figure 18: Nutrient ratios at all depths sampled during the IPY voyage.

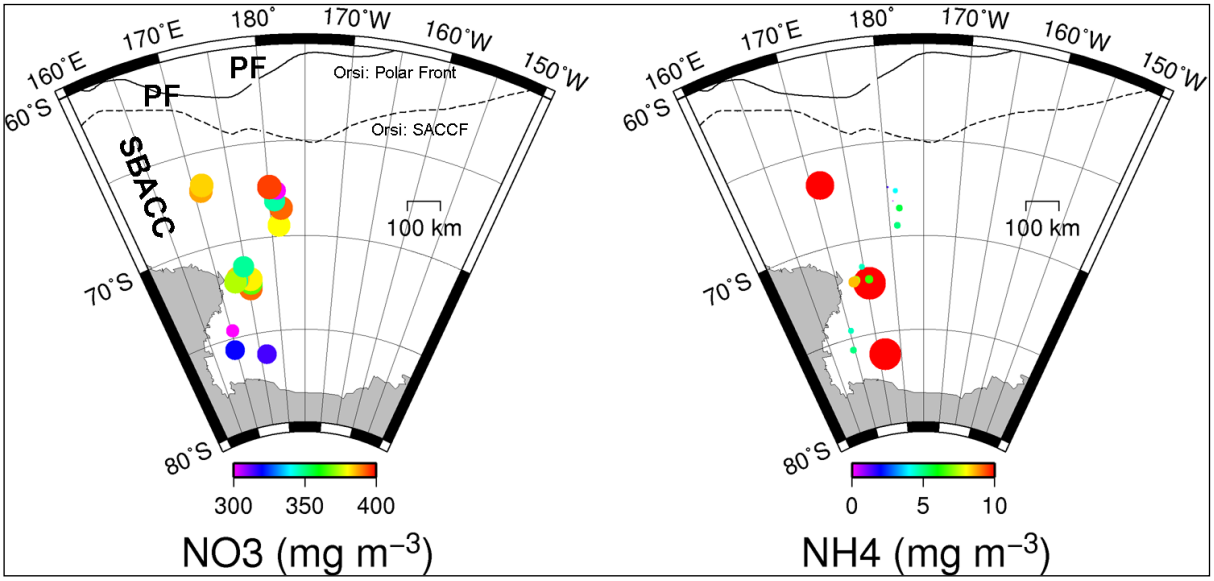

Figure 19: Surface concentrations of nitrate and ammonia.

Table 10: Physical, chemical properties and chlorophyll *a* at 20 m in the continental shelf, slope and offshore abyss, between Scott Island and the Ross Sea, during summer 2008. (Temperature in °C, salinity in parts per thousand and sigma-t in kg m^{-3})

Station	Temp.	Salinity	Sigma-t	NO_3^-	NH_4^+	DRP	µmol l^{-1} Total<2 Chl a	µg l^{-1} Chl a
Shelf								
C1	-0.791	34.197	27.542	14.29	0.29	1.19	0.77	0.01
C2	-1.500	33.854	27.289	22.00	<0.07	0.58	0.30	0.02
C3	-0.789	34.279	27.609	22.86	0.36	1.55	0.72	0.03
C4	-1.570	33.983	27.396	22.64	1.86	1.52	1.26	0.04
Slope								
C15	-1.691	33.874	27.311	30.86	1.36	1.97	0.39	0.12
C16	-1.766	33.934	27.362	25.93	2.00	1.90	0.29	0.03
C17	-1.699	34.069	27.470	26.57	0.43	1.77	0.20	0.03
C18	-1.621	34.037	27.441	28.21	0.36	1.52	0.21	0.04
C24	-1.419	33.786	27.231	27.64	0.36	1.81	0.19	0.13
C25	-1.652	34.026	27.433	29.29	0.57	1.77	0.25	0.06
C26	-1.491	33.755	27.209	21.21	0.57	1.97	0.28	0.04
C27	-1.479	34.210	27.578	25.14	0.21	1.81	0.19	0.02
Offshore								
C29*	-1.819	32.640	26.311	27.43	0.50	1.84	0.52	0.02
C30**	-1.770	33.653	27.133	27.71	0.50	1.77	0.47	0.02
C31*†	-1.616	33.658	27.133	26.29	0.14	1.48	0.41	0.02
C33**	-1.465	33.642	27.116	27.64	0.36	1.26	0.28	0.01
C34*	-0.755	33.932	27.326	28.21	0.14	1.84	0.15	0.07
C35**	-1.308	33.646	27.114	27.50	2.00	1.77	0.23	0.04

(* = Seamount; ** = Abyss; † Data from 21 m)

Classification of Water Types

Using the best-quality CTD temperature and salinity dataset, water masses were identified for all profile segments for which met acceptable standards (Table 2). In general, water masses can be identified by a distinct combination of temperature and salinity. However, in the ocean there are no distinct changes from one water mass to another. Instead, there is a gradient, usually sharp, in temperature and salinity between the different water masses. Thus even under normal conditions, there is some uncertainty in categorizing every depth sample through the water column into a distinct water mass. Where a classification was possible, the depth and relevant water masses are detailed in Table 11 below.

Table 11: Water mass classifications using WOCE-standard data, after Jacobs (2006); Jacobs & Giulivi, (1998) (see Table 2).

CTD / Core Stn. No.	Latitude	Longitude	Water Mass / Depth Range
5402 / ICOMM 55	-55.0102	174.7982	0 to 220 m: SAW
5403 / ICOMM 60	-59.9887	175.5585	0 to 220 m: CSW
5405 / ICOMM 65	-65.0062	180.0260	0 to 220 m: AASW
5411 / C15	-72.5820	175.3247	250 to 450 m: MCDW
5414 / C27	-71.9462	173.3713	0 to 150 m: AASW / 200 to 1600 m: CDW / 1700 m: AABW
5415 / C26	-72.0238	173.2553	0 to 200 m: AASW / 350 to 590 m: MCDW / 870 m: HSSW
5416 / C25	-72.0835	172.8895	0 to 275 m: AASW / 275 to 450 m: MCDW / 480 to 500 m: HSSW
5417 / C18	-71.3823	174.7483	0 to 50 m: AASW / 200 to 2000 m: CDW / 2200 m: AABW
5418 / C29	-69.4283	181.0917	0 to 100 m: AASW / 100 to 1000 m: CDW
5419 / C30	-68.5295	181.5800	0 to 100 m: AASW / 200 to 3400 m: CDW
5421 / C31	-68.1125	180.6795	0 to 100 m: AASW / 300 to 600 m: CDW
5423 / C33	-67.5980	181.1495	0 to 100 m: AASW / 400 to 3000 m: CDW
5426 / C24	-66.9818	170.8918	0 to 90 m: AASW / 200 to 450 m: CDW
5427 / C35	-66.7315	171.1773	0 to 100 m: AASW / 300 to 3000 m: CDW / 3450 m: AABW

In recent years, water mass classification has been complicated by the evidence that the characteristic temperature ranges of water masses around the Southern Ocean may be changing (M. Williams, NIWA / S. Jacobs, Lamont-Dohery Earth Observatory, pers. comm.). Figure 1 shows the general understanding of water masses and circulation in the Southern Ocean schematically, as an aid to interpretation. Figure 20 shows the T-S data for all core stations grouped into shelf, slope and deep sites. The water mass designations of Jacobs (2006) are also indicated. Figure 20 indicates a high but not unexpected degree of variability in T-S characteristics for the locations sampled.

The main oceanographic fronts in the Southern Ocean are associated with the Antarctic Circumpolar Current (ACC). From north to south, they are the Subantarctic Front (SAF), which also serves as the boundary of the Southern Ocean, the Polar Front (PF), Southern ACC front (SACCF) and the Southern Boundary of the ACC (SB). All of these fronts can split into several branches allowing for multiple crossings. Separating these effects from transient eddies is not possible, so here the mean position for this voyage is given. The Southern Ocean front separates distinct water masses. North of the SAF the surface water is Subantarctic Surface Water (SAW), while between the SAF and the PF lies Circumpolar Surface Water (CSW), and south of the PF lies Antarctic Surface Water (AASW). The SAF and PF are clearly distinguished in surface TS values measured during the voyage (Figure 15). The SAF is identified by a change in temperature from more than 8°C to less than 6°C (Sokolov & Rintoul 2007), and a change in salinity from more than 34.5 to less than 34. This places the SAF at approximately 59°S during the IPY voyage. The surface PF is defined as the maximum surface temperature gradient between 6°C and 2°C (Rintoul & Bullister, 1999). This is found at 62.5°S on the western transect and at 61.75°S on the eastern transect. South of the PF the fronts are less clear at the surface, with the SACCF being "the only Southern Ocean front that does not separate distinct water masses" (Sokolov & Rintoul 2007). Although the IPY voyage sampled a clear boundary at approximately 0 °C, which is likely to be the SB (which lies between 65.5°S and 76.0°S), all of the water south of the PF is Antarctic Surface Water (AASW). The AASW has a geographic trend in the underway data, being fresher between approximately 65°S and 70°S, and more saline in the core of the Ross Sea continental shelf. The positions of these fronts are consistent with the mean positions found by Sokolov & Rintoul (2007) using satellite-derived sea surface height measurements.

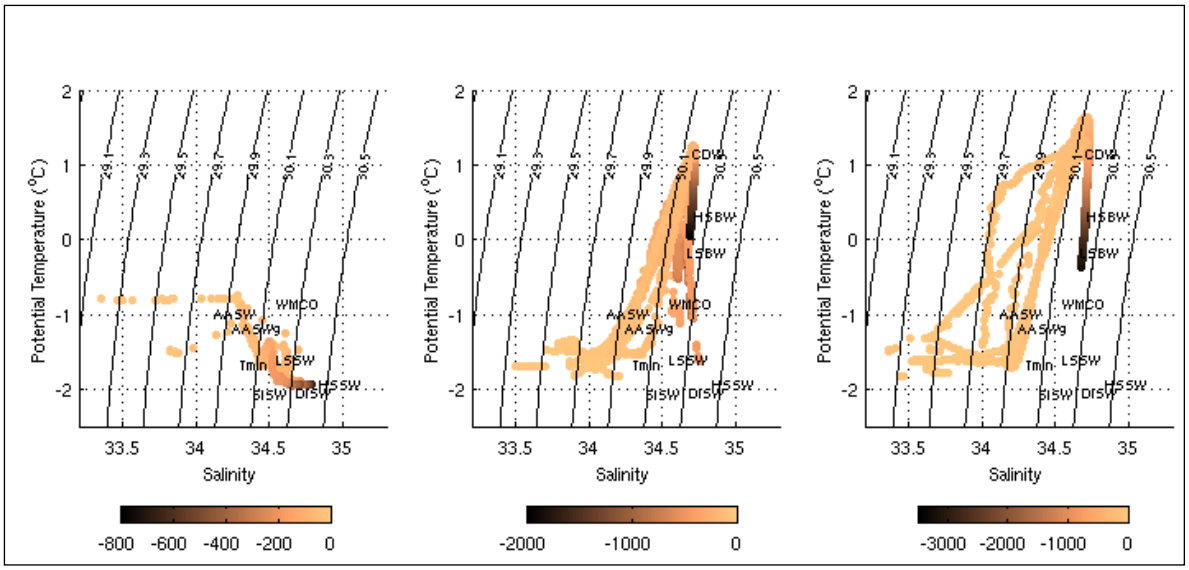

Figure 20: Water mass characteristics for the shelf, slope and deep water stations, compared with the definitions of Jacobs (2006).

Mixed layer depth

Mixed layer depths were calculated using the CTD profiles, with the mixed layer assumed to end at the shallowest case of temperature gradient exceeding 0.0075 and salinity gradient exceeding 0.0035. These cut-off parameters were chosen to achieve the smallest difference in mixed layer depth on those casts with the fewest missing data points (5414, 5415, 5416, 5426). Table 12 lists the mixed layer depth estimates from both salinity and temperature gradient analyses. One of three options is used to define the final mixed layer depth: 1) if only one tracer was available, this was used; 2) if two mixed layer depth estimates were available and were similar, then the mean value was calculated; 3) if two mixed layer depth estimates were available but were significantly different, then the value most consistent with the water column structure was chosen. The third method was applied only where either the data sparsity led to poorly defined gradients in one data set, or there was high variability in the top few metres of the cast.

CTD Station No.	Core Station No.	Date	Latitude	Longitude	Temperature-derived MLD (m)	Salinity-derived MLD (m)	Final MLD (m)
5402	ICOMM 55	3 Feb 08	-55.0102	174.7982	47	21	47
5403	ICOMM 60	4 Feb 08	-59.9887	175.5585	39	-	39
5405	ICOMM 65	6 Feb 08	-65.0062	180.0260	-	31	31
5411	C15	19 Feb 08	-72.5820	175.3247	45	-	45
5414	C27	23 Feb 08	-71.9462	173.3713	47	59	53
5415	C26	23 Feb 08	-72.0238	173.2553	39	39	39
5416	C25	24 Feb 08	-72.0835	172.8895	45	37	41
5417	C18	26 Feb 08	-71.3823	174.7483	73	19	73
5418	C29	29 Feb 08	-69.4283	181.0917	25	27	26
5419	C30	1 Mar 08	-68.5295	181.5800	45	45	45
5420	C30	1 Mar 08	-68.6335	181.6292	49	95	49
5421	C31	2 Mar 08	-68.1125	180.6795	47	33	40
5423	C33	3 Mar 08	-67.5980	181.1495	39	35	37
5426	C24	9 Mar 08	-66.9818	170.8918	61	41	51
5427	C35	11 Mar 08	-66.7315	171.1773	19	19	19

Mixed layer depths were less than 100 m across the voyage domain, suggesting strong stabilisation through surface heating. Without profiles of the light field at each station, it is impossible to conclude that light limitation of phytoplankton growth was minimal, but this is likely to be the case. Estimates of euphotic zone depth obtained by double-inversion of ocean colour data using standard NASA algorithms produced estimates which were much deeper than the MLDs (i.e. phytoplankton within the MLD were always within the euphotic zone), but the satellite data exhibited considerable spatial and temporal variability, and were not considered reliable.

3. CONCLUSIONS

The New Zealand IPY-CAML voyage (February–March 2008) covered mostly Antarctic Surface Water. Two prominent phytoplankton blooms were observed, in which nitrate:phosphate ratios were constant suggesting that nutrients were replete, yet there were some optical indications of phytoplankton senescence. . Dense, high salinity, subsurface shelf waters were sampled in only a few stations, while MCDW was sampled at all shelf and deep-water stations. The range of physical characteristics and locations of surface frontal expressions were consistent with the literature.

Passive microwave satellite data indicated that sea-ice concentrations were unusually high during both months of the voyage, compared to the nine-year mean, and a significant, though spatially variable correlation was found between ice cover anomaly and the Southern Oscillation Index.

Novel bio-optical data were gathered during the voyage. Although quality control is ongoing, particularly for the scattering measurements, a useful volume of data was collected for comparison with ocean colour satellite imagery. Unfortunately, the spatial coverage of the satellite data was severely inhibited by cloud and ice cover. The voyage dataset therefore lends itself to an examination of bias in the monthly composites of satellite-derived chlorophyll and primary production values (Schwarz et al., 2012), which are commonly used to examine primary production (e.g. Smith & Comiso 2008).

Differences between temperature and salinity data from difference-approved equipment were confounded by drifting of the ship between deployments. However, in many cases differences were less than 0.001 in both temperature and salinity, indicating that these alternative datasets yield useful information, expanding the coverage of temperature and salinity measurements. As the DTIS sensor was trawled for several kilometres on each deployment, this dataset also provides valuable information about spatial variability in temperature and salinity in the deeper water masses.

4. ACKNOWLEDGMENTS

This research was funded by the New Zealand Government under the New Zealand International Polar Year-Census of Antarctic Marine Life Project (Phase 1: So001IPY; Phase 2: IPY2007-01). We gratefully acknowledge project governance by the Ministry of Fisheries Science Team and the Ocean Survey 20/20 CAML Advisory Group (Land Information New Zealand, Ministry of Fisheries, Antarctica New Zealand, Ministry of Foreign Affairs and Trade, and National Institute of Water and Atmosphere Ltd).

5. REFERENCES

Amante, C.; Eakins, B.W. (2009). ETOPO1 1 Arc-Minute Global Relief Model: Procedures, Data Sources and Analysis. *NOAA Technical Memorandum NESDIS NGDC-24*, 19 p.

Behrenfeld, M.J.; Boss, E.; Siegel, D.A.; Shea, D.M. (2005). Carbon-based ocean productivity and phytoplankton physiology from space. *Global Biogeochemical Cycles 19*, GB1006, doi: 1029/2004GB002299.

Bowden D.; Clark, M.R.; Cummings, V.; Lörz, A-N; Maas, E.; Hewitt, J. (2011). Benthic invertebrate fauna of the Ross Sea and northern seamounts: results from the New Zealand International Polar Year – Census of Antarctic Marine Life survey 2008-2011. Final Research Report to the Ministry of Fisheries, October 2011.

Chang, F.H.; Williams, M.J.M.; Schwarz, J.N.; Hall, J.A.; Maas, E.W.; Stewart, R. (2012). Spatial variation of phytoplankton assemblages and biomass in the New Zealand sector of the Southern Ocean during the late austral summer 2008. *Polar Biology 36(3)*: 391–408.

Hanchet, S.; Mitchell, J.; Bowden, D.; Clark, M.; Hall, J.; O'Driscoll, R. (2008). Ocean Survey 20-20, NZ IPY-CAML Final Voyage Report. NIWA Client Report WLG2008-74.

Jacobs, S.S. (2006). Observations of change in the Southern Ocean. *Transactions of the Royal Society A, 364(1844),* 1657–1681. doi: 10.1098/rsta.2006.1794.

Jacobs, S.S.; Giulivi, C.F. (1998). Interannual ocean and sea ice variability in the Ross Sea. In Ocean, Ice, Atmosphere: Interactions at the Antarctic Continental Margin, ed. S.S. Jacobs & R.F. Weiss, *Antarctic Research Series 75*, AGU, Washington D.C., 135–150.

Jeffrey, S.W.; Mantoura, R.F.C; Wright, S.W. (1997). Phytoplankton pigments in oceanography.UNESCO Publishing, Paris. ISBN 92-3-103275-5

Kowalczuk, P.; Ston-Egiert, J.; Cooper, W.J.; Whitehead, R.F.; Durako, M.J. (2005). Characterization of chromophoric dissolved organic matter (CDOM) in the Baltic Sea by excitation emission matrix fluorescence spectroscopy. *Marine Chemistry 96*, 273–292.

Lovenduski, N.S.; Gruber, N. (2005). Impact of the Southern Annular Mode on Southern Ocean circulation and biology. *Geophysical Research Letters, 32*, L11603, doi:10.1029/2005GL022727.

Maas, E. (2011). Post voyage analysis of the New Zealand IPY-CAML survey of the Ross Sea, Objective 7: Micro-organisms. Final Research Report to the Ministry of Fisheries, December 2011.

Orsi, A.H.; Whitworth III, T.; Nowlin Jr., W.D. (1995). On the meridional extent and fronts of the Antarctic Circumpolar Current. *Deep-Sea Research I 42*: 641–673.

Parsons, T.R.; Maita, Y.; Lalli, C.M. (1992). A Manual of Chemical and Biological Methods for Seawater Analysis. Pergamon Press, New York, USA, 144 p.

Rintoul, S.R.; Bullister, J.L. (1999). A late winter hydrographic section from Tasmania to Antarctica. *Deep-Sea Research I 46*: 1417–1454.

Schwarz, J.N.; Kowalczuk, P.; Kaczmarek, S.; Cota, G.F.; Mitchell, B.G.; Kahru, M.; Chavez, F.P.; Cunningham, A.; McKee, D.; Gege, P.; Kishino, M.; Phiney, D.A.; Raine, R. (2001). Two models for absorption by coloured, dissolved organic matter. *Oceanologia 44(2)*: 109–241.

Schwarz, J.N; Williams, M.; Pinkerton, M.H;, Chang, H.; van Kooten, M.; Gall, M.; Cunningham, C.; Hanchet, S.; Hall, J. (2012). In situ data and monthly chlorophyll composites in the Ross Sea, austral summer 2008. Proceedings of Ocean Optics XXI, Glasgow, U.K.

Smethie, W.M.; Jacobs, S.S (2005). Circulation and melting under the Ross Ice Shelf: estimates from evolving CFC, salinity and temperature fields in the Ross Sea. *Deep-Sea Research Part I-Oceanographic Research Papers, 52(6)*: 959–978.

Smith, M.B.; Labat, J-P.; Fraser, A.D.; Massom, R.A.; Koubbi, P. (2011). A GIS approach to estimating interannual variability of sea ice concentration in the Dumont d'Urville Sea near Terre Adélie from 2003 to 2009. *Polar Science 5*: 104–117.

Smith Jr., W.O.; Comiso, J.C. (2008). Influence of sea ice on primary production in the Southern Ocean: A satellite perspective. *Journal of Geophysical Research 113*: C05S93, doi:10:1029/2007JC004251.

Sokolov, S.; Rintoul, S.R. (2007). On the relationship between fronts of the Antarctic Circumpolar Current and surface chlorophyll concentrations in the Southern Ocean. *Journal of Geophysical Research 112*, C07030. doi: 1029/2006JC004072.

Spreen, G.; Kaleschke, L.; Heygster, G. (2008). Sea ice remote sensing using AMSR-E 89-GHz channels. *Journal of Geophysical Research 113*, C02S03, doi:10.1029/2005JC003384.

Stammerjohn, S.E.; Martinson, D.G.; Smith, R.C.; Yuan, X.; Rind, D. (2008), Trends in Antarctic annual sea ice retreat and advance and their relation to El Niño–Southern Oscillation and Southern Annular Mode variability. *Journal of Geophysical Research 113*, C03S90, doi:10.1029/2007JC004269.

Stephens, C.; Schwarz, J.N.; Maas, E.; Chang, F.H.; Hall, J.; Hanchet, S. (2010). Post voyage analysis of New Zealand IPY-CAML survey of the Ross Sea: Objective 3. NIWA Final Research Report. (Unpublished report held by Ministry for Primary Industries, Wellington.)

Tassan, S.; Ferrari, G.M. (1995). An alternative approach to absorption measurements of aquatic particles retained on filters. *Limnology and Oceanography 40*, 1358–1368.

Welschmeyer, N.A. (1994). Fluorometric Analysis of Chlorophyll a in the Presence of Chlorophyll b and Pheopigments. *Limnology and Oceanography, 39(8)*, 1985–1992.

Zapata, M.; Rodriguez, F.; Garrido, J.L. (2000). Separation of chlorophylls and carotenoids from marine phytoplankton: a new HPLC method using a reversed phase C8 column and pyridine containing mobile phases. *Marine Ecology Progress Series 195*, 29 – 45.